Understanding the Glomerular Mesangium through Computational Modeling

A Dissertation
SUBMITTED TO THE FACULTY OF
UNIVERSITY OF MINNESOTA
BY

Sarah Hunt

IN PARTIAL FULFILLMENT OF THE REQUIREMENTS
FOR THE DEGREE OF
DOCTOR OF PHILOSOPHY

Victor H. Barocas, Adviser

June 2017

Acknowledgments

This thesis would not have been completed without the support of so many people. First, my committee has been amazingly patient, supportive, and helpful over my entire time in graduate school. My adviser, Victor Barocas, has consistently been both encouraging and challenging, and without his guidance I could not have finished. I am very thankful to have been part of his lab because he is so good at being a true mentor for his students. I had no idea how important his wisdom on public speaking, networking, writing, programming, modeling biology, and so much more, would be to me over the years. He has demonstrated real care for my entire wellbeing, beyond my work in the lab. Thank you. Yoav Segal has also been overwhelmingly generous with his time and attention over the years. I would not have learned so much about kidney biology and kidney disease without his help, and his insistence on remembering the big picture goal has made me a better scientist. Kevin Dorfman has also been a key adviser. His expertise has pushed the work further and deepened my theoretical base of understanding. Thank you both so much! I am very grateful to Patrick Alford for agreeing to serve on my committee, and I have enjoyed learning from him very much.

Beyond my committee, I have been supported by many other people on campus. Noro Adriamanalina's tireless efforts to support graduate students of color have been extremely helpful. The grant writing seminar she organized helped me win an NIH fellowship, and the community she supports was extremely beneficial. Thanks to Edgar Peña, Pajau Vangay, and Nancy Trejo, who kept me focused during our writing sessions.

Carolyn Scott, Shailabh Kumar, Emily Tubman, and Lazarina Gyoneva, provided essential social support over the years. I really enjoyed getting to know all of you.

Everyone in lab has helped over the years as well. Thanks to Faisal Hadi, Victor Lai, Spencer Lake, Colleen Witzenburg, Sara Jouzdani, and Tina Lenneman, who welcomed me into the lab as a new student and showed me the ropes. They have helped with countless questions over the years. Special thanks to Amy Clausen and, again, Lazarina Gyoneva who entered the lab with me. Amy always set the standard for quality presentations and pushing research forward. Inka was always up for kidney discussion and has become a very good friend. I'd also like to thank Hallie Wagner, Julia Quindlen, Chris Korenczuk, David Nedrelow, Ryan Mahutga, Emily Bermel, Vahhab Zarei, Rohit Dume, and Shannen Kizilski who both helped with the work and made working much more fun.

So many people have helped me and encouraged me over the years that I'm almost afraid to list them here because I'm sure to forget someone. But I will try: Nathan and Sarah Krampe, Nathan Shenk, Apryl and Dave Lindeman, Coley Waataja, Jenny and Dave Tesch, James and Genna Christenson, Hailey and Stephen Wilson, and Courtney Ross – your prayers and encouragement were hugely appreciated. I have leaned on your support so much, that I'm not sure how to thank you. Jenny and Courtney were amazing roommates for one year. Hailey has been a faithful friend almost since I moved to Minnesota. Angela Wu and Dahyen Kim were also awesome roommates and good friends; let's stay in touch! Amanda Adams has also been a great roommate and friend after I moved to Duluth.

I have to thank my amazing and wonderful family. My parents, Guerney and Harriet Hunt, are truly behind any success I might have. They laid a foundation, led by example, encouraged, prayed, encouraged some more, and never doubted me. Daddy, I will always be grateful for your attention, care, and affection, even when I'm not feeling super grateful at the time. Mommy, your support, teaching, and example have been so critical for so long, there's no way that I can really express how much you've done for me, and how much I love you. All of my siblings have helped and strengthened me. Ruth Burke has been an amazing example and encouragement. Ruth, your encouragement and example as a social scientist and mother have been so helpful for me. Nyron, I truly appreciate your guidance as well, and I have been so thankful to have your and Ruth's home as a second base of welcome. Anna, you have inspired me with your commitment and encouraged me numerous times. Enoque, although I haven't known you as long, I have been strengthened by your energy, excitement, and your faith. Abigail and Guerney – I can't express how much your support and care has meant over the years. I feel like we've been going through this whole process together. Abigail, you are my best friend, not just my sister. Thank you for sharing your life with me and reaching out to stay connected even though you're so far away. Guerney, even though we're seven years apart, I have been so blessed by your example, as well as your support, encouragement, prayers, and even preaching ☺. I'm looking forward to my travels with both of you, and I pray that we will always remain best friends.

Lastly, I have to thank the Lord for his work in my life. His love, faithfulness, and transformational power are the true reason that I am who I am today.

Dedication

This thesis is dedicated to my mother, Harriet Hunt. You taught me so much.

Abstract

The mesangium plays a prominent role in maintaining glomerular homeostasis by contributing to hemodynamic regulation, macromolecule clearance, and immune monitoring. However, it is also intimately involved in the development of glomerular disease. In this work we examine the physics of transport in the mesangial region by creating a computational model. This model suggests that physiological parameters play a key role in controlling the distribution of macromolecules within the mesangium. In particular, it suggests that aberrant glycosylation of IgA in IgA nephropathy may be damaging because of how it changes the Péclet number.

The model is then extended to describe transport within the glomerular tuft through the mesangial matrix. Again, we examine this transport under a range of physiological parameters. Our results suggest that transport within the mesangium may operate as one of two broad regimes – an "accumulating" regime where the mesangium provides additional filtration surface area and large macromolecules may accumulate in the region, and a "shunting" regime where the mesangium allows solutes to bypass the full length of glomerular capillary filtration

Table of Contents

List of Tables

List of Figures

C, Pé = 0.34, $\Psi = 0.071$, $\delta_{BM} = 0.1$, and $\varphi = 0.15$. 3A shows the pressure profile and convective flux of the large molecule, B shows the concentration profile and diffusive flux, and C shows the total flux of a large molecule. Here the low Péclet means that despite the high value of Ψ, little accumulation in the mesangial region occurs. Instead, the solute diffuses from the high concentration capillary (afferent) to the low concentration capillary (efferent) as seen in panel C. D-F) In panels D – F, Pé = 2.79, and $\Psi = 0.071$, $\delta_{BM} = 0.1$, and $\varphi = 0.15$. The three panels again show convective flux, diffusive flux, and total flux respectively. Here, the large Péclet number causes extensive mesangial accumulation as convection in from both capillaries dominates. G-I) In panels G-I, Pé = 0.34, $\Psi = 0.0028$, $\delta_{BM} = 0.4$, and $\varphi = 0.05$. Again, the small Péclet number results in no accumulation and the transport is diffusion dominated. J-L) In panels J-L, Pé = 2.79, $\Psi = 0.0028$, $\delta_{BM} = 0.4$, and $\varphi = 0.05$. Here, although the Péclet number is large (which caused extensive accumulation for large values of Ψ), the small value of Ψ causes a convective flow from afferent to efferent. Thus the convection-dominated transport sweeps solutes to the efferent capillary with little mesangial accumulation. (page 50)

.

Chapter 1: Introduction

The kidneys are critically important to several body functions including eliminating waste, maintaining salt balance, and regulating blood pressure. They filter the blood supply, processing about 180 L/day in humans (18). Each human kidney is composed of about one million nephrons, the unit of blood filtration and waste processing. Each nephron is composed of a glomerulus, the site of initial blood filtration, and associated tubule. A sketch of a nephron is shown in figure 1-1, with the kidney glomerulus in the upper left. The glomerulus is a spherical network of fenestrated glomerular capillaries. High hydrostatic pressure within the glomerular capillaries drives filtration across the capillary walls. The glomerular filter consists of the fenestrated endothelium, the basement membrane on which the endothelial cells sit, and interdigitated podocytes, which are specialized epithelial cells on the capillary exterior. Blood plasma and small solutes pass through this filtration process and enter the urinary space surrounding the glomerulus. This initial filtrate then enters the tubule, where it is further processed, before exiting the nephron as urine.

This work focuses on the glomerulus, and in particular on the role of a glomerular substructure, the mesangium. Outlined in hatched gray in figure 1-2, the mesangium is centrally located in the glomerulus, and intimately connected with the fenestrated endothelium (77, 79). Composed of resident smooth-muscle-like mesangial cells and their associated matrix (mesangial matrix), the mesangium is directly involved in both maintaining glomerular health and in the pathogenesis of glomerular diseases. The mesangium provides structural support for the glomerular capillaries, communicates with

endothelial cells and podocytes, assists in regulating glomerular hemodynamics, and clears dead cells and macromolecules that accumulate in the region. Additionally it is involved in the pathogenesis of multiple glomerular diseases, including IgA nephropathy, membranoproliferative glomerulonephritis, and diabetic nephropathy (20).

Mesangial cells provide the necessary structural support that closes the glomerular capillary loop. Mesangial cells insert into the basement membrane (GBM), and develop contractile microfilament bundles that hold opposite sides of the GBM against intracapillary pressure (49, 77). Experimental models that directly injure or lyse mesangial cells have shown that when mesangial cells fail, glomerular capillaries may balloon, microaneurysms can develop, and, in the most extreme case, glomerular architecture may be lost completely (49, 60, 94). Even models that only disrupt mesangial cells' mechanical attachments to the GBM, but leave them otherwise functional, will alter glomerular hemodynamics by increasing glomerular filtration, most likely through expansion and additional filtration in the mesangial region (49).

Mesangial cells are also involved in continual cross-talk with the other glomerular cell types. Mesangial cells rely on endothelial production of PDGF-B to grow and persist, and loss of endothelial cells results in mesangial cell death (79). Additionally, mesangial cells and podocytes produce chemokines that can bind to each other's receptors (79). Beyond mesangial-podocyte and mesangial-endothelial communication, mesangial cells also possess gap junctions (96), and are contiguous with the extraglomerular mesangium (59, 95). Extraglomerular mesangial cells have a demonstrated role in tubuloglomerular feedback (TGF) (75). The intraglomerular mesangium's electrical connection to this

structure raises the possibility of extraglomerular to intraglomerular mesangial communication and involvement in TGF.

There is support for a mesangial role in hemodynamic regulation. After experimental mesangial cell lysis, the glomerular ultrafiltration coefficient is reduced and GFR falls (93). Normal glomerular filtration rate (GFR) and capillary pressure responses to plasma volume expansion (PVE) are also lost; glomeruli without mesangial cells do not increase SNGFR in response to PVE (6). Glomerular response to angiontensin II (Ang II) administration is attenuated in the absence of mesangial cells – Ang II administration does not decrease SNGFR (6). In culture, mesangial cells contract in response to Ang II (89), but the connection to the observed hemodynamic behaviors *in vivo* has not been established.

Multiple tracer studies have demonstrated that large molecules or nanoparticles preferentially accumulate within the mesangial region (14, 28, 29, 48, 57, 84). Mesangial cells may phagocytose these molecules to some extent (58), but an additional clearance route runs from within the glomerular mesangium to the extraglomerular mesangium, followed by secretion into the proximal tubule (53). The mesangium also has a resident population of myeloid dendritic cells (59) with strong phagocytic propensities, and mesangial cells themselves possess immunoglobulin receptors (26, 59, 80). The mesangial environment thus presents an ideal location for monitoring overall blood composition. Key analytes accumulate in the region, and it is intimately connected with the structures controlling glomerular filtration (JGA and macula densa).

The mesangium thus assists in maintaining homeostasis in healthy glomeruli. However, disease can disturb these maintenance processes, resulting in progression of the disease rather than resolution. The mesangium responds early to glomerular diseases (9, 36), and one initial indicator is often mesangial proliferation and matrix deposition (1). Exogenous TGF-β can stimulate extracellular matrix deposition in mesangial cells (8). Activation of mesangial cells by immune complexes results in the release of several interleukins, tumor necrosis factor (TNF), reactive oxygen species, and extracellular matrix deposition (20, 59, 70). Clearly, mesangial cells can have strong pro-inflammatory effects. Additionally, there is a small subpopulation of immunologically active cells that seem to permanently reside in the mesangium (20). When activated, these cells, in combination with activated mesangial cells, can then attract invading macrophages (70). All of this inflammatory activity and mesangial matrix expansion leads to stiffening of the glomerulus, and potentially to podocyte death, which in turn may lead to complete loss of glomerular function (59).

All of this research reveals the mesangium's critical role in maintaining glomerular health, and its contribution to the progression of glomerular disease. However, our understanding of filtration and solute transport in the mesangial microenvironment remains incomplete. In contrast, filtration through the glomerular capillary wall has been well studied both *in vivo* and computationally. The ability to measure glomerular filtration rate either for the whole subject (85) or in a single nephron (17) has allowed characterization of the filtration process under many different conditions. The work of Deen and colleagues (21, 27, 64) has afforded major theoretical insights into aspects of

transport across the glomerular capillary wall. Since a vast majority of the plasma filtration occurs through the capillary wall rather than through the mesangium, these studies have provided little information about mesangial transport, but they have helped to create an accurate vision of the glomerular capillary milieu.

The major focus of this work is on modeling the physical mechanisms behind the mesangium's maintenance of homeostasis and contribution to disease progression. The aim is to 1) describe the underlying physics of mesangial transport, and 2) examine the influence of physiological parameters on that transport. A model of transport in the mesangium may explain the observed macromolecule accumulation in the region. The model is also extended to include the larger context of the glomerular tuft. The mesangium's central location suggests that plasma flowing through the mesangial matrix could bypass glomerular filtration, and solutes might move through the region from the afferent to the efferent capillary. We develop a model to account for this flow and examine what physiological conditions influence the mesangium's ability to concentrate key solutes (amplifying a signal for sensing) or to bypass filtration.

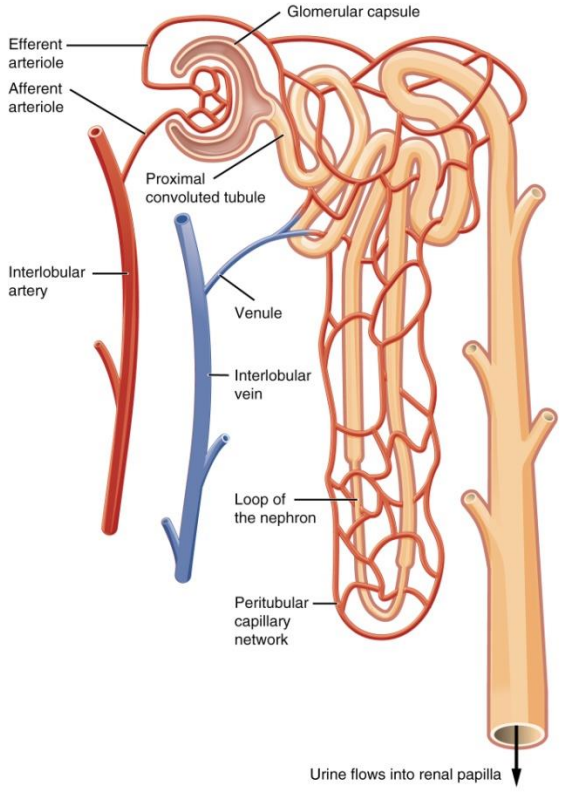

Figure 1-1: A diagram of a kidney's nephron. Initial blood filtration takes place in the glomerular capsule. The filtrate formed then enters the proximal tubule, and is processed through the loop of the nephron. Urine flows out the collecting duct. Used with permission from (99). Download for free at http://cnx.org/contents/14fb4ad7-39a1-4eee-ab6e-3ef2482e3e22@8.81

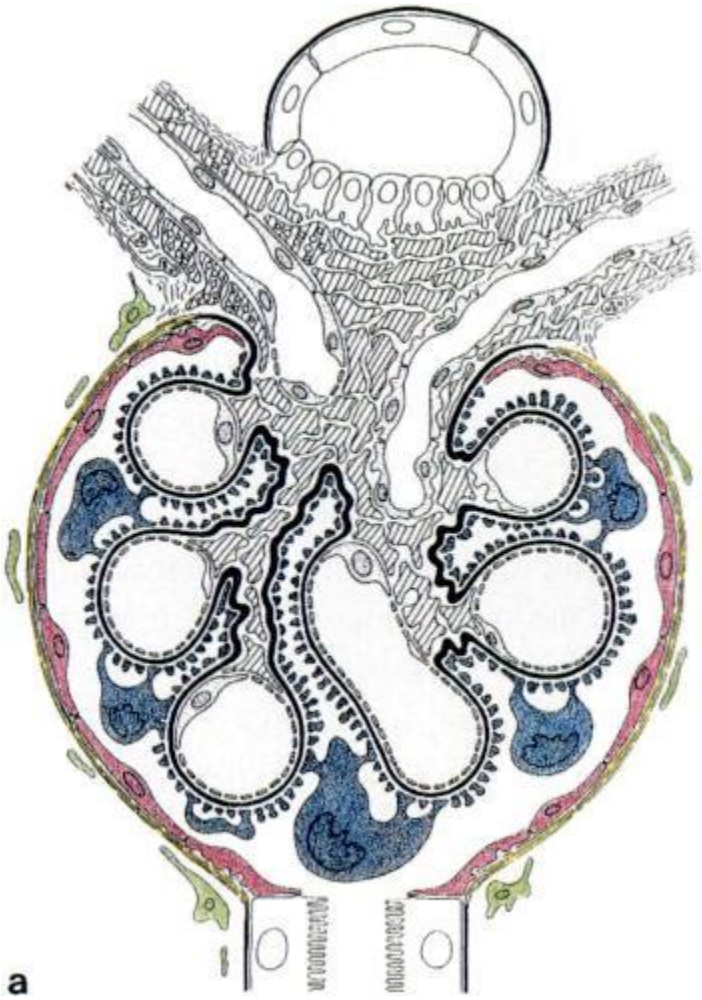

Figure 1-2: Cross-sectional sketch of a glomerular capillary. The mesangium occupies the central portion, drawn in the hatched gray. The blue cells are the specialized epithelial cells, podocytes. The basement membrane is outlines in thick black, and the endothelial cells are shown as the fenestrated lining of the capillary lumens. Republished with permission of JASN, from (44); permission conveyed through Copyright Clearance Center, Inc

Chapter 2: Modeling mesangial accumulation in IgA nephropathy

This chapter is part of the manuscript:

Hunt, S. E., Dorfman, K. D., Segal, Y., & Barocas, V. H. (2016). A computational model of flow and species transport in the mesangium. *American Journal of Physiology-Renal Physiology*, *310*(3), F222-F229.

2.1 Summary

As discussed in the introduction, a variety of macromolecules accumulate in the glomerular mesangium in many different diseases. In this chapter we studied the physics of the transport of these molecules within the porous mesangial matrix, using a computational model of convection and diffusion, and we applied this model to the specific instance of immunoglobulin A (IgA) transport in IgA nephropathy. We examined the influence of physiological factors including glomerular basement membrane (GBM) thickness and mesangial matrix density on the total accumulation of IgA. Our results suggested that IgA accumulation can be understood by relating convection and diffusion, and that the relative strength of these effects depend strongly on intrinsic glomerular factors.

2.2 Introduction

The objectives of this chapter were 1) to develop a computational model of plasma and species transport within the mesangium, and 2) to apply that model to the question of how different factors contribute to the mesangial accumulation of IgA in IgA

nephropathy. IgA nephropathy may be considered archetypal; the disease, which has been associated with a number of different contributory/causative factors (2, 5, 37, 45, 61, 62, 92), hinges upon aberrant biodistribution, with the defining symptom being accumulation of IgA in the mesangium. The key result of our analysis is the recognition that IgA nephropathy may be considered in terms of the transport of IgA, whereupon many disparate physiological states can be attributed to changes in the Péclet number governing the relative effects of convective transport in flow to diffusion of IgA.

Glossary

a Radius of diffusing molecule

a_1, a_2 Osmotic pressure coefficients

c_{alb} Albumin concentration

D_0 Free diffusion coefficient, calculated from the Stokes-Einstein equation

D_{alb} Diffusion coefficient of albumin

δ_{PFB} Thickness of the filtration barrier (basement membrane + podocytes)

k_B Boltzmann constant

$K_{D,mes}$ Hydraulic conductivity of the mesangial matrix $K_D = \kappa/\mu$

$K_{D,PFB}$ Hydraulic conductivity of the perimesangial filtration barrier

κ Tissue Darcy permeability

μ Plasma viscosity

λ Ratio of molecule radius to fiber radius

p Hydrostatic pressure in the mesangium

p_{ext} Hydrostatic pressure in Bowman's space

Π Oncotic pressure in mesangium

$\vec{n}$ Surface normal vector

φ Fiber volume fraction, in mesangial matrix or perimesangial filtration barrier (PFB)

r Matrix fiber radius

T Temperature (K)

$\vec{v}$ Plasma velocity

2.2 Materials and Methods

Species transport in the mesangium is governed by convection due to plasma flow, diffusion due to chemical gradients, and reaction with other extracellular components and/or removal by the cells. For the present model, only convection and diffusion were considered. Importantly, the plasma flow rate depends not only on the mechanical pressure but also on the oncotic pressure, which in turn is determined largely by the albumin concentration (65). As a result, our model had three components: plasma flow, albumin transport, and IgA transport. The three components are described below.

Plasma flow model.

Plasma flows through the mesangial matrix and composite perimesangial filtration barrier (PFB), which represents the composite resistance from the glomerular basement membrane and the podocyte layer. The average pore size in the mesangium is ≈ 20 nm (53), forcing a low flow rate where inertial effects are negligible. Furthermore, since the pore size is very small compared with mesangial dimensions of 1–3 mm (42, 77), the

problem may be further simplified to Darcy flow, governed by:

$$\vec{v} = -K_{D,mes}\nabla p \quad \textbf{0.1}$$

$$0 = \nabla \cdot (K_{D,mes}\nabla p) \quad \textbf{0.2}$$

Here, $\vec{v}$ is the superficial velocity, $K_{D,mes}$ is the hydraulic conductivity of the mesangium, and p is the local pressure. The Darcy model has been used to describe interstitial flow in many tissues (13, 24, 51, 71, 87). Hydraulic conductivities for the mesangial matrix and filtration barrier were calculated as $K_D = \kappa/\mu$, where μ is the viscosity of plasma, and κ is the tissue's Darcy permeability. Two different permeabilities were used, one for the mesangium to calculate $K_{D,m}$, and one representing the resistance of the PFB to calculate $K_{D,PFB}$, the perimesangial filtration barrier hydraulic conductivity. Permeability was calculated from fiber radius (r) and fiber volume fraction (φ) (15):

$$\kappa = \frac{3r^2}{20\phi}(-\ln\phi - 0.931) \quad \textbf{0.3}$$

Boundary conditions on equation 2.1 were (see figure 2-1):

- The pressure in the capillary was defined to be the baseline pressure and set to 35 mmHg.
- The hydrostatic pressure in Bowman's space was set to 1.3 mmHg, (i.e., 33.7 mmHg below the average glomerular capillary pressure). At the filtration barrier boundary, the plasma flux was determined by the combination of oncotic and hydrostatic pressure (24).

$$\vec{n} \cdot \vec{v} = -K_{D,mes}\frac{\partial p}{\partial y} = \frac{-K_{D,PFB}}{\delta_{PFB}}(p - p_{ext} - \Pi) \quad \textbf{0.4}$$

Here, $\vec{n}$ is the surface normal, $\vec{v}$ is the velocity, δ_{PFB} is the filtration barrier thickness, $K_{D,PFB}$ is the hydraulic conductivity of the filtration barrier, p is the hydrostatic pressure in the mesangium, and p_{ext} is the hydrostatic pressure in Bowman's space. $K_{D,PFB}$ was calculated using equation 0.3, with values of r (2 Å) and φ (0.3) chosen to achieve reasonable mesangial flux rates (mesangial flux can only be a small fraction of single nephron glomerular filtration rate (SNGFR) (49).

- Albumin in the filtering plasma increases the fluid's oncotic pressure relative to Bowman's space as it is well known to do in the glomerular capillary (21). The oncotic pressure was calculated from the local concentration of albumin, c_{alb} using an approximation to the Landis-Pappenheimer equation (63).

$$\Pi = a_1 c_{alb} + a_2 c_{alb} \quad \textbf{0.5}$$

Here c_{alb} is the concentration of albumin, and a_1 and a_2 are constants (listed in table 2-1). Because our model requires a diffusion coefficient which depends on size, albumin was used instead of total protein concentration in the osmotic pressure calculation. The albumin concentration (4 g/100 mL) is much higher than the IgA concentration in the plasma (0.2 g/100 mL), so IgA did not contribute to the oncotic pressure in most simulations. In cases with large accumulation of IgA, however, IgA concentrations can become significant.

- All other boundaries had zero flux, representing either a symmetry condition or an impermeable barrier. The symmetry condition on the right hand boundary (fig 2-1 B) represents the case where a second capillary is connected to the mesangial

region. We assumed the mesangial cell was impermeable to flow, leading to a no flux condition on the bottom boundary.

Albumin Transport Model

Albumin movement within the mesangium is modeled by the convection-diffusion equation, which describes the movement of molecules in a flow field,

$$\nabla \cdot (D_{alb} \nabla c_{alb} - c_{alb} \vec{v}) = 0 \quad \textbf{0.6}$$

The albumin transport model is coupled to the plasma flow model because the flow field depends on the albumin concentration through equation 0.5, and albumin concentration depends on the flow field through equation 0.6. Therefore, these equations had to be solved simultaneously. In equation 0.6, $\vec{v}$ is the velocity obtained from equations 0.1 and 0.2, D_{alb} is the diffusion coefficient of albumin in the mesangial matrix, and it was assumed that there was negligible hindrance of albumin convection through the matrix. We calculated diffusion coefficients based on the size of the albumin molecule, and the pore size and fiber thickness of the mesangial matrix, using established models of diffusion through porous fibrous matrices (equation 0.7) (3).

$$D_{alb} = D_0 e^{-\pi \phi^b} e^{-0.84 f^{1.089}} \quad \textbf{0.7}$$

$$b = 0.174 \ln \frac{59.6}{\lambda}$$

$$f = (1 + \lambda^2)\phi$$

$$D_0 = \frac{k_B T}{6\pi\mu a} \quad \textbf{0.8}$$

Here, D_0 is the free diffusion coefficient for the molecule, φ is the volume fraction occupied by the fibers, and λ is the ratio of the molecule radius (a) to radius of the fibers in the matrix. The boundary conditions for albumin transport were as follows:

- The albumin concentration was constant at 4 g/100 mL (11) in the capillary (figure 2-1).
- The basement membrane was assumed to be a perfect filter, so the total flux across the filtration barrier was zero. In this case, $\vec{v} = 0$ because water exits the mesangial matrix across the filtration barrier. Thus, the boundary condition was

$$D_{alb}\vec{n} \cdot \nabla c_{alb} - c_{alb}\vec{n} \cdot \vec{v} = 0 \quad \textbf{0.9}$$

- All other surfaces have symmetry boundaries, so the total flux is zero on those as well. In this case, however, there is zero velocity as well ($\vec{v}$ = 0), as described above, so

$$D_{alb}\vec{n} \cdot \nabla c_{alb} = 0 \quad \textbf{0.10}$$

IgA Transport Model

The convection-diffusion equation also describes the movement of IgA complexes.

$$\nabla \cdot \left(D_{IgA}\nabla c_{IgA} - c_{IgA}\vec{v}\right) = 0 \quad \textbf{0.11}$$

Diffusion coefficients were calculated using the diameter of monomeric and dimeric IgA, in fiber matrices with varying fiber thicknesses and fiber volume fractions. Because IgA is several times larger than albumin, its diffusion coefficient is significantly smaller. The boundary conditions for IgA transport were:

- Constant concentration in the capillary of 0.2 g/100 mL (32)
- No flux from all other surfaces, noting as in the case of albumin that the plasma velocity is zero at the impenetrable surfaces, but not zero at the filtration boundary.

Implementation

A standard Galerkin finite element simulation was developed in Matlab and used to solve all equations. Linear basis functions were used on a 25,000 element mesh that was generated with rectangular brick elements, with a spacing of 0.1 μm into the depth of the mesangium, 0.01 μm along the height of the mesangium, and 1 μm along the length of the glomerular capillary. Each element had eight Gauss points, and the dimensions of the entire mesangial matrix region (figure 2-1) were 5 x 0.5 x 10 μm. A segregated solving scheme was used that first solved the Darcy flow problem, assuming zero concentrations for albumin, to output a pressure field. That pressure field was then used to calculate a velocity input to the convection-diffusion equation. This resulted in a new concentration distribution for albumin and IgA, and this concentration distribution was used to calculate an osmotic pressure. The osmotic pressure was fed back to the Darcy solver in the boundary condition, and the process iterated until the pressure solution stopped changing within a tolerance of 0.001. The results of this process were pressure at each node, and the concentrations of albumin and IgA at each node. Simulations were run on computers at the Minnesota Supercomputing Institute (MSI) on 4 processors. The problem was solved in three dimensions, but with no variation in the third direction, so concentration and velocity profiles are shown in two dimensions.

Case Studies

Our reference case was normal glomerular capillary blood pressure (35 mmHg) (86), basement membrane thickness (δ_{bm} = 0.4 μm (52)), basement membrane fiber radius of 2.0 Å and basement membrane volume fraction of 0.3, and IgA concentration of 0.2

g/100 mL (32). From this case, we examined the effects of a thin basement membrane (δ_{bm} = 0.1 – 0.3 μm (52)) and decreased IgA diffusion coefficient (increased molecular radius). We also examined the effect of mesangial matrix structure (increasing the mesangial matrix fiber volume fraction) since the deposition of mesangial matrix is a common response in glomerular disease (36). For the simulations in this study only mesangial fiber thickness was changed, with total fiber density kept constant.

Parameters in the model were varied as follows:

- Four different thicknesses of basement membrane were used: 100, 200, 300, and 400 nm.
- Mesangial matrix had a volume fraction of 0.05, 0.08, 0.1, 0.13 and 0.15, with a fiber radius of 2 nm.
- The radius of IgA was set to 75 Å, and then 1.25 and 1.5 times this number.

In addition, we also examined the effect of a reaction at the surface of the mesangial cell. In this case the boundary conditions for IgA were altered to simulate a pseudo-first-order reaction. The flux was set equal to a constant reaction rate, k, multiplied by the local IgA concentration. The reaction rate was varied among the values 1.38, 0.138, and 0.0138 μm/s, based on published in vitro studies.

2.3 Results

Results from our reference case are shown in figure 2-3. Pressure is highest at the capillary, decreasing into the mesangium due to plasma loss into the urinary space (fig. 2-3A). The pressure gradient drives flow into the mesangium and across the filtration

barrier (fig 2-3B). Transmesangial flow concentrates albumin by 1% (fig. 2-3C) and IgA by 20% (fig. 2-3D) in the mesangial interior, compared to capillary levels. Because the perimesangial filtration barrier in our model perfectly filters albumin, an oncotic pressure arises in the mesangium (fig. 2-3E) which opposes the hydrostatic pressure driving filtration. Thus, the flow (determined by pressure gradients) drives solute concentration, which in turn affects flow by altering the driving pressure.

Mesangial flux changes with both filtration barrier thickness, as well as mesangial matrix permeability (fig. 2-4). Thinner filtration barriers have the largest effect, as they decrease the resistance of the entire mesangial region (fig. 2-4A). In contrast, changing the permeability of the mesangial matrix has little effect for thicker filtration barriers (fig. 2-4B). However, at the thinnest filtration barrier tested (100 nm), mesangial matrix permeability is important. With the thinner filtration barrier, the resistance to flow from the mesangial matrix begins to approach the resistance from the filtration barrier, so changing mesangial matrix permeability has a significant influence on mesangial matrix flux.

We investigated the effects of intrinsic glomerular factors on IgA accumulation. IgA accumulation increases dramatically with thinner basement membranes (fig. 2-5A), reaching values of 10 - 100x the serum concentration, in sharp contrast to the 1.2x concentration seen in the reference case. The larger mesangial fluxes due to thinner basement membranes (fig. 2-4) carry more IgA into the mesangial region. Because of IgA's small diffusion coefficient, this increased convective flux creates steep counteracting concentration gradients and thus much higher total accumulation. IgA

accumulation also increases with increasing mesangial matrix fiber volume fraction (fig. 2-5B). As the fiber volume fraction increases, the permeability of the mesangial matrix drops. Lower permeability under a constant pressure drop causes smaller mesangial fluxes (fig. 2-4B); simultaneously, the increased matrix density results in more hindrance to diffusion. These two effects compete, with lower convective fluxes tending to decrease accumulation, but more hindered diffusion tending to increase accumulation. The net result is increased IgA accumulation as the matrix volume fraction increases (fig. 2-5B). Dimerizing IgA increases its radius and has a similar effect on diffusion, but not on flow (fig. 2-6), because the IgA concentration is so low it does not affect viscosity or osmotic pressure. As the radius of IgA increases, it becomes harder for it to move through the porous mesangial matrix, and thus its accumulation increases dramatically.

When a cell surface reaction at the fastest rate was added to the model, accumulation decreased or ceased altogether, depending on the rate of reaction. We investigated simple first-order reaction kinetics, which increase linearly with increasing substrate (IgA) concentration. For large reaction rates (k=1.38 μm/s), this resulted in the unreasonable result of a total absence of IgA accumulation (not shown). However, at lower reaction rates (k=0.138, and 0.0138 μm/s), accumulation still occurred but at lower amounts, depending on mesangial flux (fig. 2-7). In these cases, higher mesangial flux convected more IgA into the mesangium, which counteracted the loss from mesangial cell surface reaction. At lower fluxes, with k=0.138 μm/s, the reaction removed IgA more quickly than it could accumulate. For the lowest k value tested (0.0138 μm/s), IgA accumulated for all PFB thicknesses.

These results indicate that several different factors influence IgA mesangial accumulation, including perimesangial filtration barrier thickness, mesangial matrix permeability, and the radius of the diffusing IgA. These glomerular and species factors can be examined in terms of the way they affect convection and diffusion. Fundamentally, our model is a convection-diffusion model, so the importance of these factors lies in how they change convection and/or diffusion. Higher mesangial fluxes, which convect IgA, tend to increase accumulation. Higher diffusion coefficients, which allow the immunoglobulin to escape into the capillary, tend to decrease accumulation. Thus thinner PFBs, which allow increased mesangial flux, would tend to increase accumulation. Larger IgA radii, which decrease diffusion, also tend to increase accumulation.

The relative importance of convection and diffusion are quantified by the Péclet number. The Péclet number is defined as vL/D where v is a characteristic velocity, L is a characteristic length scale, and D is the diffusion coefficient. The numerator, vL, quantifies the strength of convection while the denominator, D, quantifies the strength of diffusion. For our simulation results we calculated a Péclet number using the mean velocity at the entrance of the mesangium for v, the length of the mesangium towards the symmetry boundary for L, and the diffusion coefficient of IgA for D. Plotting the accumulation of IgA vs. the Péclet number (fig. 2-8) collapses all of the case studies in this work into a single curve. This general effect was also seen in the presence of a reaction on the mesangial cell surface (fig. 2-7), but as the reaction rate got larger, IgA removal by cell surface reaction became the dominant factor.

2.4 Discussion and Conclusions

Although there is uncertainty in the specific parameter values used in this study, experimental measurements of blood velocity in the glomerular capillaries (98), mesangial dimensions (77), immunoglobulin and albumin diffusion coefficients (12, 16), mesangial pore sizes (88), and glomerular pressure drops suggest that transport in the mesangium is indeed near a Péclet number of order one. When the Péclet number is near one, convection and diffusion exert equal influence. As a result, even small changes to the strength of convection and/or diffusion, can greatly alter IgA transport. IgA accumulation will be highly sensitive to biological changes that result in increased or decreased plasma velocity or IgA diffusion, as shown schematically in Table 2-2.

The solute-agnostic nature of the model here, combined with the universality of the underlying physical principles, suggests that any macromolecule or tracer that is large or considerably hindered by the mesangial matrix will concentrate in the mesangium. Lipoproteins fall within this size range, and thus their transport would be affected by the parameters varied here (filtration barrier thickness, mesangial matrix permeability, etc.). Lipoproteins have been implicated in kidney disease (40, 90), and studies have shown that lipoprotein concentrations can affect mesangial cell proliferation (66). Tracer studies with imposil and carbon have shown that the mesangium is an important clearance route (28, 48). Size-dependent accumulation in the mesangium has also been experimentally observed (14).

A similar process appears to occur in amyloid disease of the kidney (23), with abnormal proteins (e.g., serum amyloid A protein (30)) exhibiting elevated serum levels

and subsequently concentration and fibrogenesis in the mesangium. In collagenofibrotic glomerulopathy (25), the species in question is an atypical collagen III molecule, but the mesangial accumulation is similar. Although the subsequent accumulation process and molecule-cell interactions vary with disease, and the model parameters would vary with molecule, it appears that the fundamental mechanisms explored herein are at work in many cases, and that the transport dynamics of the mesangium render it particularly vulnerable to diseases of macromolecular accumulation.

Thus, we must conclude that the well-established tendency of macromolecules to accumulate in the mesangium (78) can be explained in terms of non-specific transport phenomena. This natural accumulation may be valuable in the healthy kidney, allowing the mesangium to function as sensitive monitor of serum proteins and to use its contractility to maintain proper glomerular function (78) or communicate changes is serum protein levels to the extraglomerular mesangium and juxtaglomerular apparatus via gap junction connections (96). In the case of disease, however, this tendency to accumulate macromolecules has a negative effect on mesangial function. Thus, the general transport processes must be considered in conjunction with the specific biological processes (e.g., cell-molecule interactions) to create a full picture of a mesangial disease.

Early investigations suggested a role for the mesangium in regulating glomerular capillary diameter (7), but later work demonstrated that large capillary size changes would not result from mesangial contraction (50). Nevertheless, mesangial cell contraction can change the surrounding matrix structure: contraction will increase the space available for plasma flow while maintaining constant fiber volume, thus decreasing

matrix fiber volume fraction (68). This drop in fiber volume fraction could have significant effects on macromolecule accumulation, as the increased permeability allows easier transport across the mesangial region. Since the mesangium connects adjacent glomerular capillaries, increased capillary to capillary transport may play a role in the attenuated responses to Ang II observed after mesangial cell injury (6).

In the case of IgA nephropathy, certain factors are known to increase the risk of developing disease (92) without completely predicting it. Our model suggests that the association of thin basement membranes (TBM) with IgA nephropathy (19) might be due to TBM causing increased convection, which increases the IgA accumulation (fig. 2-4). Our model also provides insight into the findings that mesangial IgA deposition requires the presence of both IgA and soluble CD89 (sCD89) (5). Because smaller macromolecules more easily escape the mesangium (fig. 2-6), a IgA-sCD89 complex would concentrate significantly more than either IgA or sCD89 alone. Nephropathy development might hinge upon the decreased diffusion coefficient that results from complex formation and creates high mesangial concentrations.

The transport model described here is simplified, as it ignores uptake by mesangial cells, which is important in IgA nephropathy and other diseases (79). Uptake could be added to the current modeling framework by introducing a reaction term at the mesangial cell surface (i.e., by modifying the boundary condition to allow flux into the cell).Such a change to the model would lead to other dimensionless groups, comparing the rate of reaction at the cell surface to convective or diffusive transport. Since mesangial cells rapidly clear many solutes (28, 29, 41), this dimensionless number may

be more important than the Péclet number. This model only considered the accumulation of IgA. In reality, accumulation per se is not sufficient to cause damage (92), but it is a necessary step in the process. Another simplification of the model was the assumption of no solute flux into the urinary space. Albumin is known to cross the filtration barrier (35), and if IgA also leaked across the filtration barrier, that would decrease accumulation. An extended model using estimated sieving coefficients for albumin and IgA at the filtration barrier (27) could address this issue.

Parameters used in the model	Meaning	Value
μ	Plasma viscosity	7×10^{-4} Pa·s (91)
a_1	Osmotic pressure coefficient	1.63 mmHg/(g/dL) (63)
a_2	Osmotic pressure coefficient	0.294 mmHg/(g/dL) (63)

Table 2-1: Constants used in the model. Numbers in parentheses are references.

Physiological Change	Diffusion	Convection	Péclet number	IgA Accumulation
Thinner basement membranes	-	↑↑	↑↑	↑↑
Denser mesangial matrix	↓↓	-/↓	↑↑	↑↑
Larger IgA radius	↓↓	-	↑↑	↑↑

Table 2-2: Different physiological changes can have similar effects on IgA accumulation if their effect on the Péclet number is similar

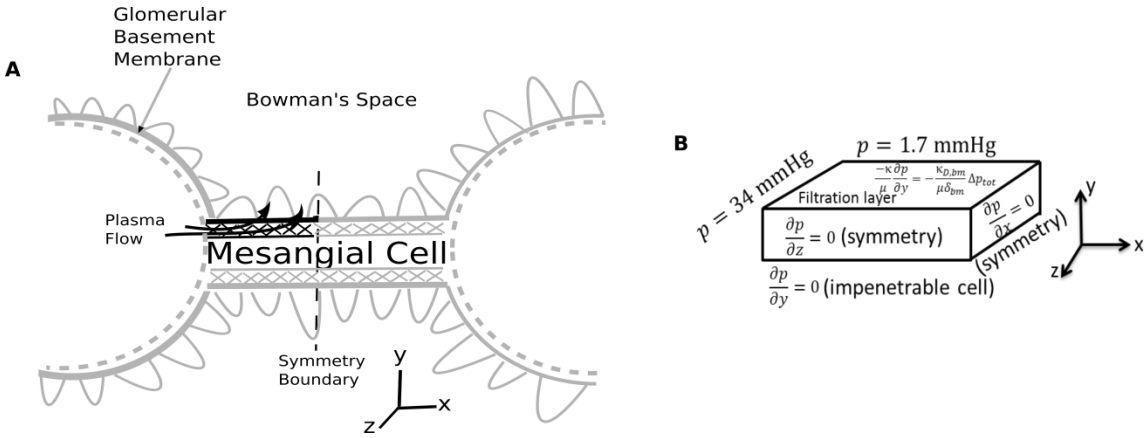

Figure 2-1: *A*: A sketch of glomerular capillaries with the adjacent mesangium. The simulation region is highlighted by dark black lines. The glomerular capillary was considered as a boundary condition. Only the mesangial matrix domain is shown in the figures. The perimesangial filtration barrier (PFB) was considered as the combination of the glomerular basement membrane and the podocytes. *B*: sketch of the simulation domain showing the pressure boundary conditions.

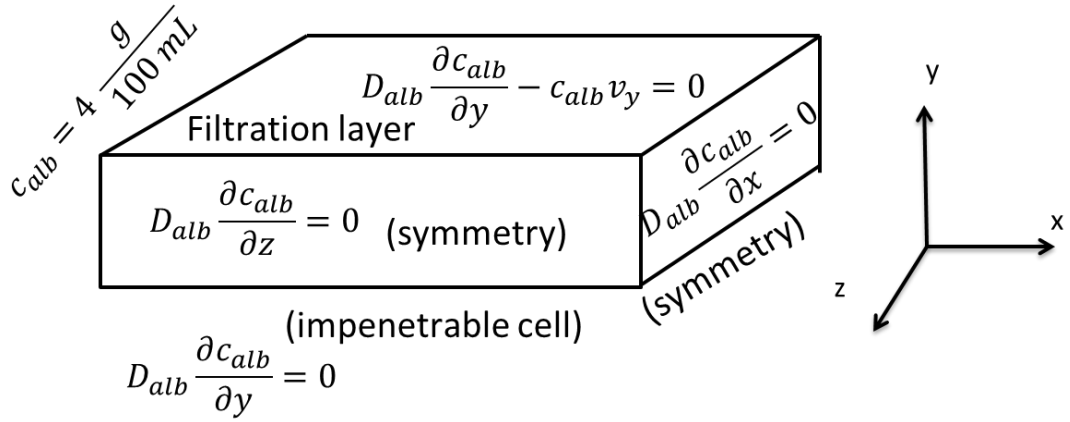

Figure 2-2: Albumin boundary conditions showing capillary concentrations on the left, with symmetry conditions on the right as well as front and rear faces. Albumin flux across the top (PFB) is defined to be zero.

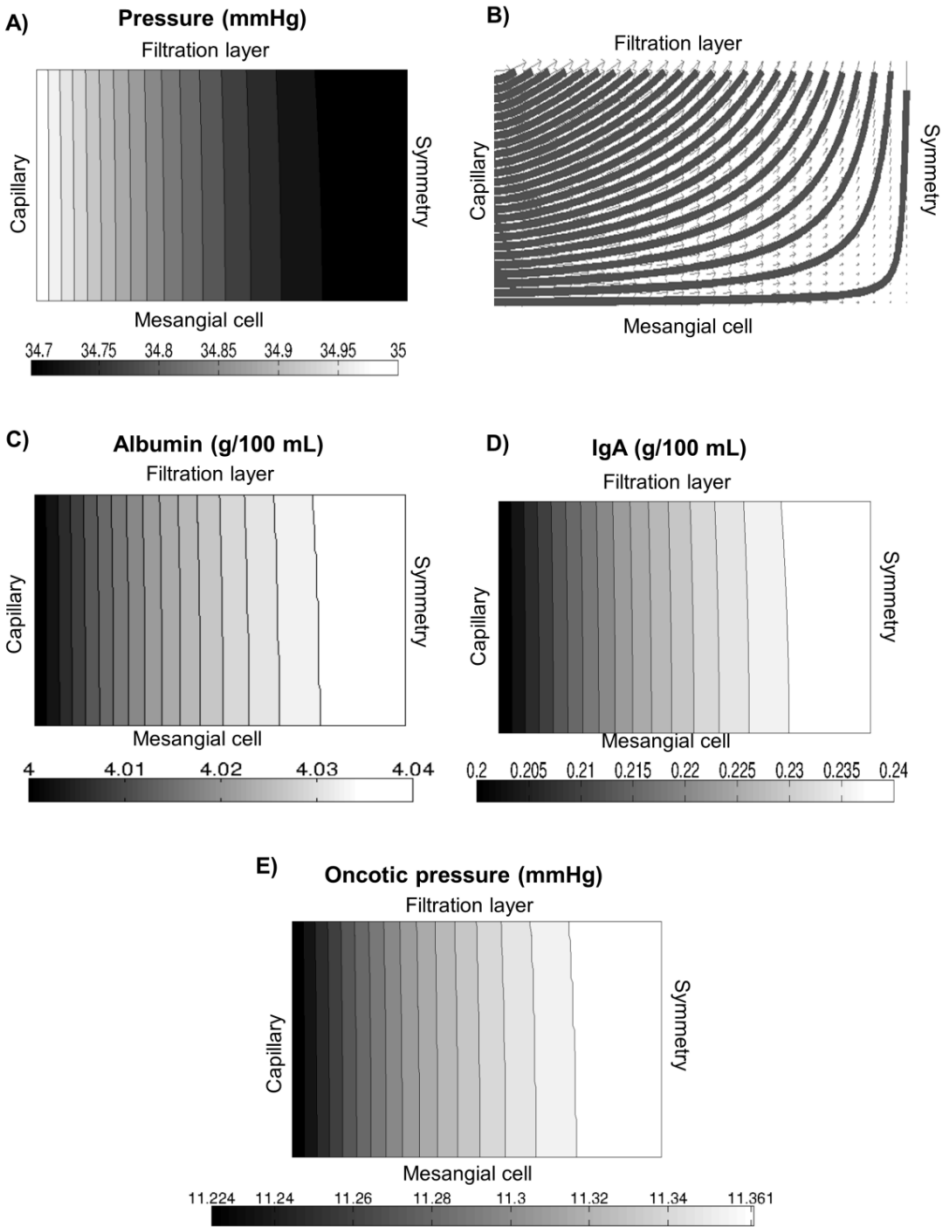

Figure 2-3: Results for the base case with a filtration barrier thickness of 0.4 µm, volume fraction φ_m= 0.05, and r_{IgA} = 75 Å. A: contour lines for the pressure in mmHg. The highest pressures are found at the capillary boundary, with the pressure quickly dropping as fluid is lost across the filtration barrier. B: streamlines of plasma flow in the mesangial matrix. The symmetry boundary condition on the right-hand side causes a sharp turn in plasma flow. C: Albumin concentration within the matrix. Albumin is very close to the plasma level throughout the mesangium. D: immunoglobulin A (IgA) concentration within the mesangial matrix. Because of its larger size, IgA diffuses more slowly and therefore concentrates more than albumin, rising 20% above its capillary concentration. E: oncotic pressure due to albumin in the mesangial matrix. This pressure significantly reduces the driving force of filtration.

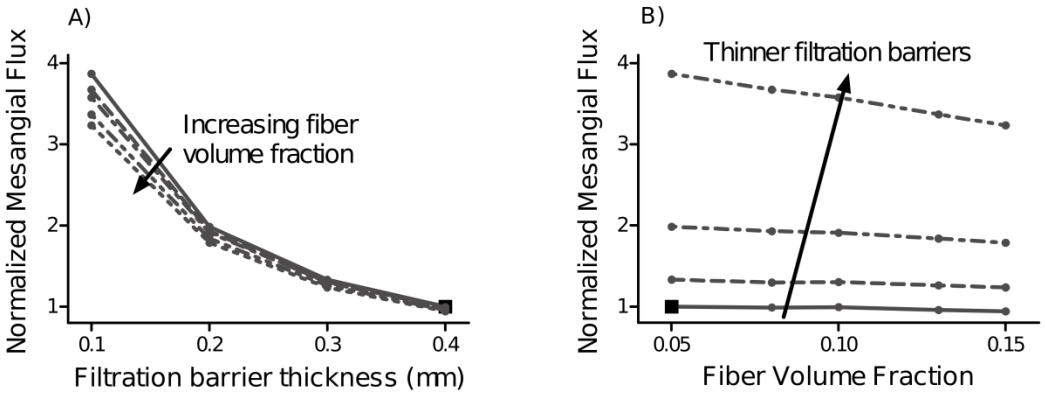

Figure 2-4: *A*: as the filtration barrier becomes thinner, mesangial flux increases. Mesangial flux values are normalized by the value in the reference case. *B*: mesangial matrix fiber volume fraction has only a small effect for thicker filtration barriers (0.2– 0.4 μm). For a filtration barrier thickness of 0.1 μm, however, changing the mesangial matrix volume fraction has a noticeable effect.

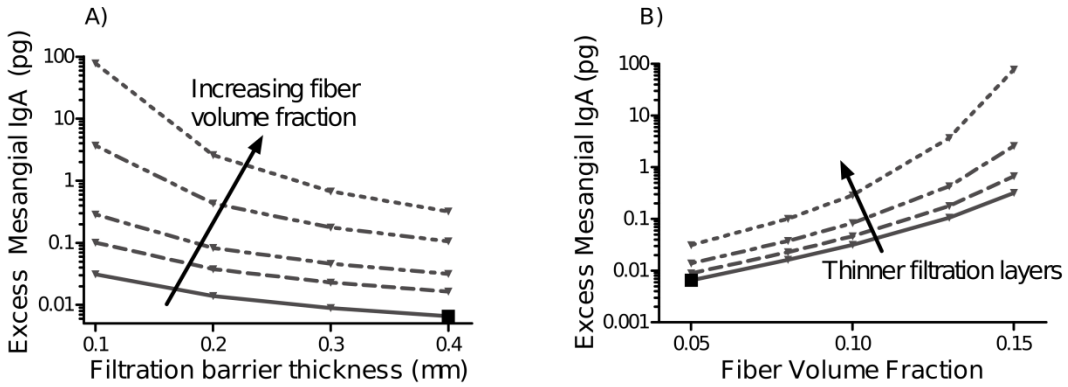

Figure 2-5: Excess mesangial accumulation vs. filtration barrier thickness (A) and mesangial matrix fiber volume fraction (B). Excess mesangial IgA is the IgA in the mesangial matrix above the concentration in the capillary. The reference case is again marked with the large black square.

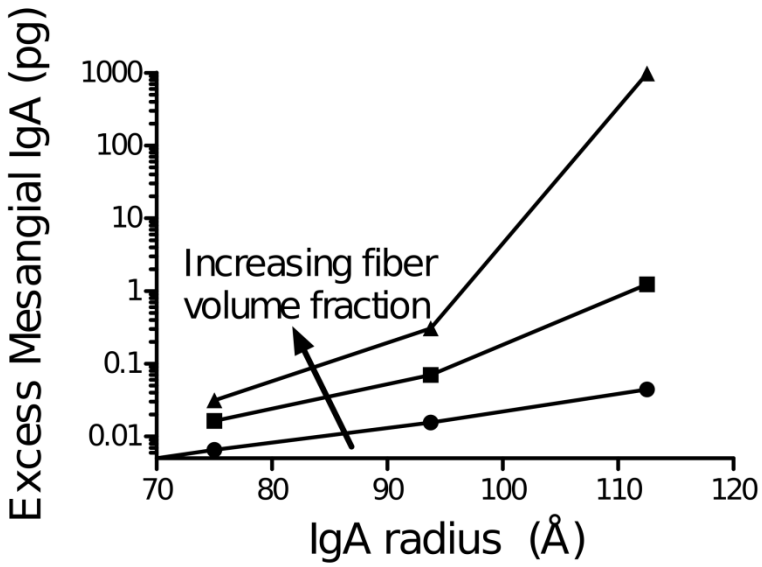

Figure 2-6: As the radius of IgA increases, the accumulation of IgA in the mesangium also increases. Results shown here are for IgA having a radius of 1x, 1.25x, and 1.75x, the actual radius of IgA. These results are with a filtration barrier thickness of 0.4 μm, and mesangial matrix volume fractions of 0.05, 0.08, and 0.1.

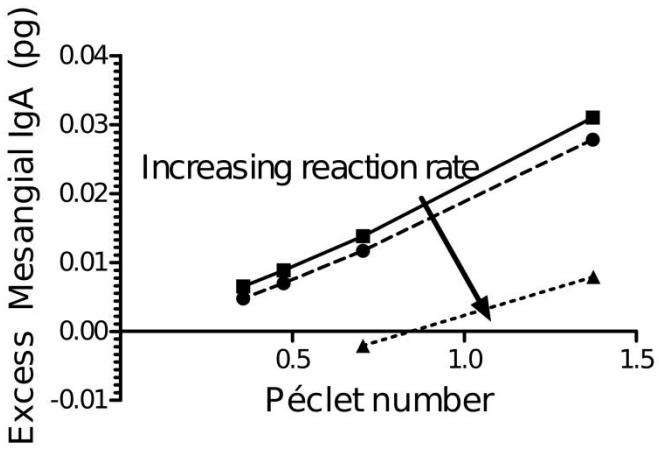

Figure 2-7: When a cell surface reaction is added to the model accumulation decreases. The magnitude of the decrease depends on the reaction rate, with faster reactions leading to less accumulation or even eliminating it altogether.

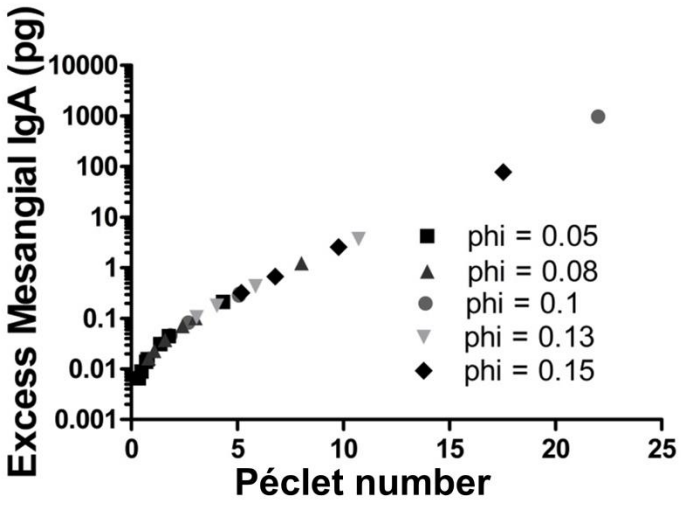

Figure 2-8: The accumulation of IgA in the mesangium for the cases plotted earlier but vs. the Péclet number. They form a smooth line, suggesting that accumulation depends significantly on Péclet number rather than the specific parameters of the simulation.

Chapter 3: Mesangial transport in the context of the glomerular tuft

This chapter is part of the manuscript:

Hunt, S. E., Dorfman, K. D., Segal, Y., & Barocas, V. H. The mesangium as a shunt and a sensor. Submitted to *Physiological Reviews*.

3.1 Summary

Building on the work presented in the previous chapter, we extended our model to focus on the potential role of the mesangium in sensing overall blood composition. We created a model of the mesangium situated between two counter-currently flowing glomerular capillaries, and explored macromolecular accumulation under varying glomerular conditions. This work demonstrated that the mesangium can act as a shunt, allowing plasma and solutes to bypass glomerular capillary filtration, and as an accumulator, accumulating macromolecules to concentrations above their capillary level.

3.2 Introduction

The mesangium's previously discussed functions in maintaining homeostasis, involvement in inflammation, and connection to the JGA, all suggest a role for the mesangium as a process monitor within the larger control system for glomerular filtration and blood homeostasis. Any exploration of this potential role must begin, however, with an understanding of the movement of analytes within the mesangial microenvironment. The mesangium abuts the glomerular capillaries, and is open to flow from the capillary lumen through the fenestrated endothelium (46, 47). Analyses of whole glomeruli have shown that the mesangium connects capillary segments to each other and also to the

urinary space via filtration across the mesangial basement membrane (39). Two consequences of this structure arise. First, plasma flowing through the mesangium can bypass afferent to efferent filtration in the capillary, effectively shunting the flow. Second, this flow convects large, slowly diffusing molecules into the mesangial matrix, where they accumulate to concentrations above their capillary levels (47, 48), facilitating sensing. In this we work we create a finite element model to examine how such a shunt sensor system might operate. We identify a range of physiologically reasonable conditions under which transport within the mesangium concentrates extremely dilute solutes in the blood, i.e., amplifies the signal that would be sensed by receptors on mesangial cells.

Glossary

a_1, a_2 osmotic pressure coefficients

c_{alb} concentration of diffusing albumin

D_{alb} diffusion coefficient of albumin

h thickness of mesangial channels

$\vec{J}_{mes}$ net flux into mesangial region

k permeability of capillary wall

κ Darcy permeability of the mesangial matrix

μ plasma viscosity

$\vec{n}$ surface normal vector

P_U pressure in the urinary space

P_{UF} net ultrafiltration pressure

p hydrostatic pressure

Q volumetric flow through capillary

S capillary surface area

$\vec{v}$ plasma velocity

3.3 Materials and Methods

The complicated geometry of the glomerular capillaries was simplified as shown in figure 3-1. Capillaries were modeled as straight cylinders, with the abutting mesangium occupying a constant amount of surface area. The blood in the capillaries was assumed to be well mixed over the capillary cross-section, so concentrations at the mesangial surface were equal to bulk concentrations in the capillary. In order to model both capillary and mesangial transport, capillary volumetric flows and the resulting capillary concentrations were first calculated along a one-dimensional line following the capillary's axis. Changes in volumetric flow down the length (afferent to efferent) of the capillary due to filtration were calculated based on (81):

$$\frac{dQ}{dz} = -kSP_{UF} \quad \textbf{3.1}$$

Here Q is the volumetric flow rate, k is the permeability of the capillary wall, S is the filtration surface area of the capillary wall, and P_{UF} is the net ultrafiltration pressure, which will be defined below. For an isolated capillary (i.e., one without a mesangium), the mass flow rate of a solute that cannot pass through the filtration barrier must remain constant, which results in

$$\frac{d(Qc)}{dz} = c\frac{dQ}{dz} + Q\frac{dc}{dz} = 0$$

where c is the concentration of the solute of interest. Combined with equation 3.1, equation 3.2 implies that

$$\frac{dc}{dz} = -\frac{c}{Q}\frac{dQ}{dz} = \frac{kcSP_{UF}}{Q} \quad \textbf{3.3}$$

The constant mass flow rate (M) allows us to write $Q = \frac{M}{c}$. This relationship is used with equation 3.3 to make an initial estimate of the albumin profile for the capillary, where the concentration of interest is c_{alb}. The pressure $P_{cap}(z)$ along the capillary length was specified as a small linear pressure drop, and the net ultrafiltration pressure P_{UF} was calculated as:

$$P_{UF} = P_{cap} - P_U - a_1 c_{alb} - a_2 c_{alb}^2 \quad \textbf{3.4}$$

In equation 3.4, P_U is the urinary pressure and a_1 and a_2 are constants used to calculate the oncotic pressure (63, 74). Given an inlet volumetric flow (Q_0), initial albumin concentration ($c_{0,alb}$ = 5.8 g/dL (10)), and urinary pressure (P_U is 34 mmHg below capillary pressure), equations 3.3, and 3.4 allow us to calculate the albumin concentration profile for the isolated capillary. Once the albumin profile is calculated, the same equations can be used to calculate the concentration profile for any solute of interest.

We used a segregated solving scheme for the coupled capillary-mesangium problem. First, equations 3.1 and 3.5, (shown below), were solved for the capillary to calculate a concentration profile and volumetric flux along the capillary. Next, the capillary concentration and pressure profiles were passed as boundary conditions to the mesangial matrix model. The pressure and concentration in the mesangial region were then calculated via an extended version of the method previously described (38). Briefly,

plasma flow through the mesangial region was assumed to be governed by Darcy's law for an incompressible fluid (eq. 3.5), with pressure depending on the mechanical and osmotic pressure differences between the mesangium and the urinary space.

$$\nabla \cdot \vec{v} = \nabla \cdot \left(-\frac{\kappa}{\mu} \nabla p \right) = 0 \quad \textbf{3.5}$$

In equation 3.5 μ is the plasma viscosity and κ is the Darcy permeability of the mesangial matrix. Darcy permeabilities were calculated based on the volume fraction of fibers in the mesangial matrix and the radius of those fibers as in (38).

Transport of solutes was governed by the convection-diffusion equation (eq. 3.6), and all solutes were assumed to have free access from the glomerular capillaries into the mesangial region (valid for solutes less than 40.5 nm in mean length (46)).

$$\nabla \cdot (D_{alb} \nabla c_{alb} - c_{alb} \vec{v}) = 0 \quad \textbf{3.6}$$

In equation 3.6 D_{alb} is the hindered diffusion coefficient of albumin, estimated using established models of diffusion through porous fibrous matrices (38). The computed mesangial region pressure and concentration profiles were then used to calculate the plasma flux ($\vec{J}_{mes}$) into (or out of) the adjacent capillaries:

$$\vec{J}_{mes} = -2\vec{n} \left(\frac{\kappa}{\mu} \nabla p \right) \Big|_{mes-cap} h \quad \textbf{3.7}$$

In equation 3.7, h is the height of the mesangial matrix, p is the pressure in the matrix, and $\vec{n}$ is the surface normal unit vector. The factor of 2 results from the geometry shown in figure 3-1, with two mesangial regions for each capillary. These fluxes were combined with the capillary filtration in the mass balance on plasma to yield an update to equation 3.1:

$$\frac{dQ}{dz} = -(kSP_{UF} + \vec{j}_{mes}) \quad \textbf{3.8}$$

Combining equation 3.7 with equation 3.8 results in

$$\frac{dQ}{dz} = -kSP_{UF} + 2\vec{n} \cdot \left(\frac{\kappa}{\mu}\nabla p\right)\Big|_{mes-cap} h \quad \textbf{3.9}$$

Equation 3.9 describes the plasma flow (Q). The flux of solutes into/out of the mesangium was also calculated:

$$\vec{j}_{solute}|_{mes} = \left(-D\nabla c - c\frac{\kappa}{\mu}\nabla p\right) \cdot \vec{n} \quad \textbf{3.10}$$

Here, D is the diffusion coefficient for the solute in question, and c is the solute concentration. For a capillary without an adjacent mesangium, the solute flow along the capillary, Qc, would be a constant. However, for a capillary with a mesangium that is open to fluid flow, solutes can be lost or gained through flux from the mesangium. The solute concentration equation (equation 3.3) then becomes:

$$\frac{d(Qc)}{dz} = 2h\vec{n} \cdot \left(D\nabla c + c\frac{\kappa}{\mu}\nabla p\right)\Big|_{mes-cap} \quad \textbf{3.11}$$

Equations 3.9 and 3.11 were solved simultaneously to get c(z), the protein profile along the capillary length. This concentration profile was then used as a boundary condition on the mesangial matrix, and the process was iterated until the solution had converged (within 0.001).

To represent countercurrent flow, a linear pressure drop in the positive z-direction was specified as a boundary condition on one side (the afferent side) of the mesangial matrix, while a linear pressure drop in the negative z-direction was specified on the opposite (efferent) side of the mesangial matrix. Input concentrations of albumin and IgA were set on the afferent side. Then the pressure and concentrations at the entrance to the efferent side were set equal to the pressure and concentrations at the exit from the

afferent side. The characteristics of mesangial transport were examined for solutes ranging in size from an overall radius of 47 to 98.25 Å.

3.4 Results

Flow and Pressure Field

The large-scale nature of mesangial transport depends strongly on fundamental physiological parameters. Figure 3-3 shows the streamline and pressure profiles for two contrasting cases, selected to demonstrate different parametric regimes. Figure 3-3A shows streamlines for a basement membrane thickness of 0.4 μm and matrix volume fraction of 0.05. Here, the blood plasma flows from the afferent capillary through the mesangial matrix to the efferent capillary. In this case, the loose mesangial matrix, in combination with the high resistance to flow from the thick basement membrane, acts as a shunting channel, providing a conduit for the movement of solutes and water from one capillary to another. This shunting slightly raises the solute concentration in the efferent capillary, and lowers it in the afferent, but the effect is small (~10%). Figure 3-3B shows the streamlines for a basement membrane thickness of 0.1 μm and a mesangial matrix volume fraction of 0.15. In this case, the thin basement membrane provides low resistance to plasma entering the urinary space, and the thicker matrix obstructs intercapillary flow. As a result, plasma enters the mesangium from both capillaries and exits across the basement membrane into the urinary space. In this situation the mesangial matrix provides additional filtration surface area, beyond that of the glomerular capillary walls.

This dramatic difference in streamline profiles results from the interaction between two different resistances to flow: the basement membrane and the mesangial matrix. The basement membrane resists fluid flow more than the mesangial matrix in all cases, but as the resistance of the mesangial matrix increases towards that of the basement membrane, plasma moves into the mesangial interior from both capillaries and then filters through the mesangial basement membrane, as shown in figure 3-4A,D. In contrast, when the resistance from the mesangial matrix is far below that of the basement membrane, shunting flow (as shown in figure 3-4G,J) results. The relative resistance between these two flow paths can be captured by the dimensionless ratio $\Psi = \frac{\kappa_{BM} L_{mes}}{\kappa_M \delta_{BM}}$. In figure 3-4A-F, we had $\Psi = 0.071$, whereas figure 3-4G-I was calculated for $\Psi = 0.0028$.

Species Distribution

The factor Ψ, which is large if the basement membrane is highly permeable and the mesangium is not, clearly affects distribution of solutes within the mesangium. In addition, because there are both convection and diffusion within the mesangium, the Péclet number (vL/D), which captures the relative contributions of convection and diffusion, must also play a role. Concentration profile results for four limiting cases are shown in figure 3-4. In that figure, the molecular size of the transported species was adjusted to maintain consistent Péclet numbers for panels A-C, G-I and C-D,J-L.

Figure3- 4A-C (the *shunting* case) shows the streamlines for plasma flow (3-4A), the diffusive (3-4B) and convective (3-4C) species fluxes, and the concentration of a large

molecule in the case where the basement membrane is thick (0.4 μm), and the mesangial matrix is loose ($\varphi = 0.05$). The loose matrix allows an effective diffusion coefficient of ≈ 4.1 $\mu m^2/s$, but the convective fluxes still dominate the overall transport of material (Figure 3-4C). As a result, the convection sweeps large molecules through the mesangium, and they do not accumulate to high levels. The concentration in the mesangial matrix is only 5% above the bulk concentration in the capillary.

In contrast, figure 3-4D-F (the *accumulating* case) shows the mesangial concentrations with a thin basement membrane (0.1 μm) and dense mesangial matrix ($\varphi = 0.15$). Here, the effective diffusion coefficient is reduced due to hindering, maintaining a fairly large Péclet number (Pé = 2.79) in spite of the reduced flow rates. As seen in figure 3-4D, the convective fluxes from both the afferent and efferent capillaries carry material into the mesangium, and diffusive fluxes move out of the mesangial region to both afferent and efferent capillaries to maintain the system at equilibrium. The net result of the diffusive and convective influence is a very low magnitude movement from efferent to afferent and high accumulation in the mesangial region, with concentrations reaching four times the circulating plasma levels.

In contrast, solutes whose transport is governed by diffusion (Péclet numbers less than one) move from the high concentration capillary (afferent) to the low concentration capillary (efferent) (figure 3-4A-C,G-I) . For both values of Ψ in this column, large solutes do not accumulate, but rather recirculate within the capillary loop, opposite of convection.

Since diffusion dominates under these conditions, the ideas of shunting and accumulation do not apply. Rather, the species simply diffuse across the mesangium because of the slight concentration difference between the afferent and efferent capillaries.

3.4 Discussion

The most significant result of this work is the identification of different functional regimes within the possible parameter space of mesangial transport. In particular, we have identified some situations ("shunting") in which the mesangium could potentially allow plasma and species to move from an afferent to an efferent arteriole without passing through the full length of glomerular capillary filtration. In other situations ("accumulating"), however, the mesangium acts as additional filtration surface area, beyond that provided by the capillary walls, and can accumulate species.

Shunting occurs when the basement membrane is thick and the mesangial matrix is loose. Under these conditions, the mesangial matrix provides a pathway of little resistance to fluid flow, and the basement membrane resists filtration into the urinary space. Because of the loose mesangial matrix, species carried by the flow can easily enter and exit the mesangial space. This flow does not appear to have a significant impact on capillary concentrations, which are much more sensitive to filtration across the glomerular capillary wall. Binding to mesangial cell receptors were not considered in this model, but such reactions are well established (29, 31, 34, 90). In the presence of mesangial cell binding, concentrations in the mesangial interior could change significantly, and the shunting flow could become important.

The more interesting case is that of accumulation. When the basement membrane is thin and the mesangial matrix is dense, plasma and solutes move from both the afferent and efferent capillaries into the mesangial interior. Here, the mesangium provides additional filtration surface, with plasma being filtered across the mesangial basement membrane. The dense matrix highly hinders the diffusion of solutes, particularly large solutes, which causes a dramatic increase in their concentrations in the mesangium. Thus the mesangium could be extremely sensitive to even small changes in the circulating plasma concentrations of key analytes. Consistent with this idea, multiple studies have established the movement of tracers and molecules from the circulation into the mesangial matrix (28, 29, 41, 48, 53). Evidence also shows that the mesangium reacts early in the progress of glomerular disease (36, 59, 80). Our results shed light on the physiological conditions that may lead to mesangial response.

Mesangial cells exist in a unique microenvironment, and can react to a combination of molecular signals (67, 82, 86), mechanical cues (33, 55, 76, 97), and/or electrical signals(69, 86, 96). Based on the current work, it is possible for analyte concentrations in the mesangium to reach several times those in the circulating plasma, which could be extremely important in terms of molecular signal processing. If the cells in the mesangium are serving as sensors to monitor the blood's health (83), then the mesangial architecture could act as an amplifier to provide those sensors with the highest possible signal-to-noise ratio. The amplification would be favorable both in the case of mesangial cells contributing to the maintenance of hemeostasis, and in the case of

immune cells reacting to inflammatory cues (4, 78). Furthermore, accumulation of species could facilitate clearance by the mesangial cells (20, 48, 54, 56).

.

Parameter	Meaning	Value
a_1	Osmotic pressure constant	1.63 mmHg/(g/dL)(74)
a_2	Osmotic pressure constant	0.294 mmHg/(g/dL)^2(74)
h	Mesangial channel width	0.5 μm (estimated) (43, 77)
μ	Plasma viscosity	1.35 x 10^{-3} Pa·s (91)
P_U	Urinary space pressure	34 mmHg below capillary pressure (10)
Q_0	Initial volumetric plasma flow rate	8.3 x 10^5 μm^3/s (22)
R	Capillary radius	5 μm (72)
$c_{0,alb}$	Initial concentration of albumin	5.8 g/dL (10)

Table 3-1: Values for constants used in the model. Numbers in parentheses are references.

Figures

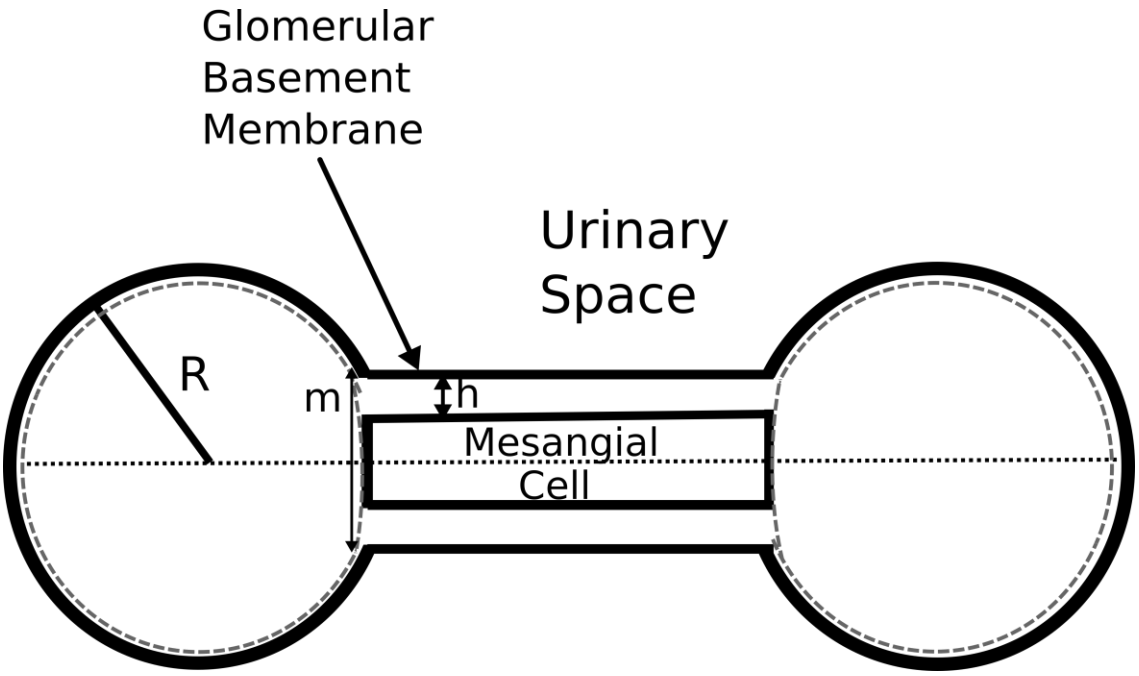

Figure 3-1: A sketch of the geometry used in the model. R is the capillary radius, m is the width of the entire mesangial region, and h is the width of the mesangial matrix channels. The central rectangle represents the impermeable mesangial cell, and the dashed line is a line of symmetry used to simplify calculations.

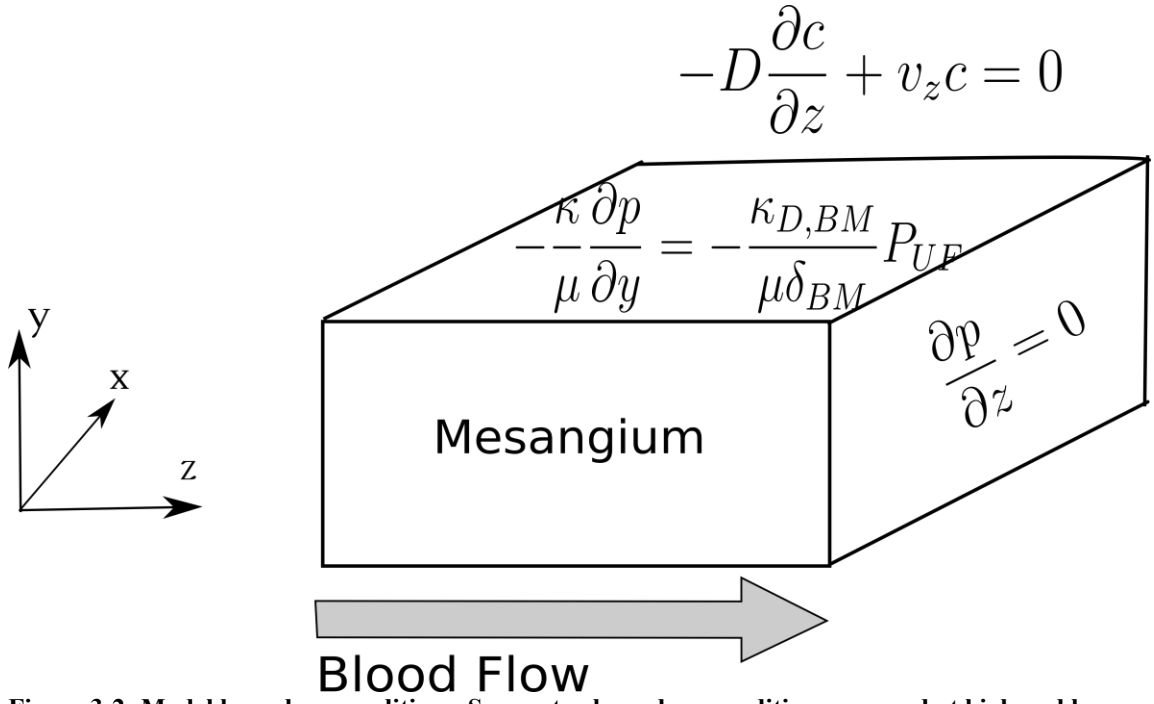

Figure 3-2: Model boundary conditions. Symmetry boundary conditions are used at high and low values of z. Plasma filters across the basement membrane, but it is completely impermeable to solutes.

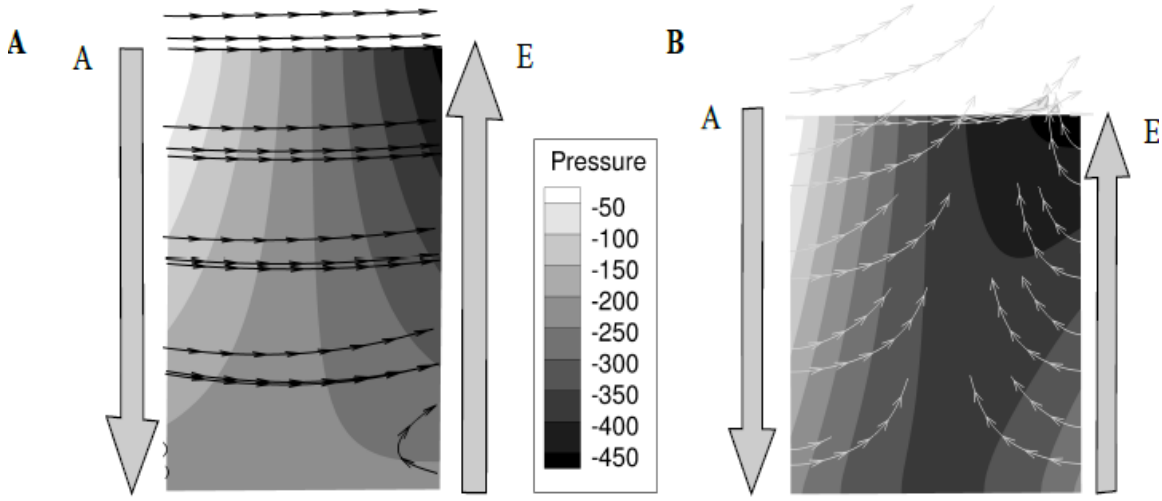

Figure 3-3: Plasma flow streamlines through the glomerular mesangium between an afferent (A) and an efferent (E) capillary for two different cases. Streamlines terminate when they hit the mesangial boundary. A) Plasma streamlines for the case where δ_{BM} =0.4 µm and φ_m = 0.05. Here, the thick basement membrane has a high resistance to filtration into the urinary space. In combination with a loose mesangial matrix, plasma shunts from the afferent capillary to the efferent capillary, with relatively little crossing into the urinary space. In this situation the mesangial matrix acts as a channel for fluid to move from the afferent to the efferent side. B) Flow for the case where δ_{BM} =0.1 µm, and φ_m = 0.15. Here, a thinner basement membrane offers much less resistance to filtration into the urinary space. Combined with the high resistance to inter-capillary flow offered by the dense mesangial matrix, plasma quickly begins to filter into the mesangium from both the afferent capillary and the efferent capillary.

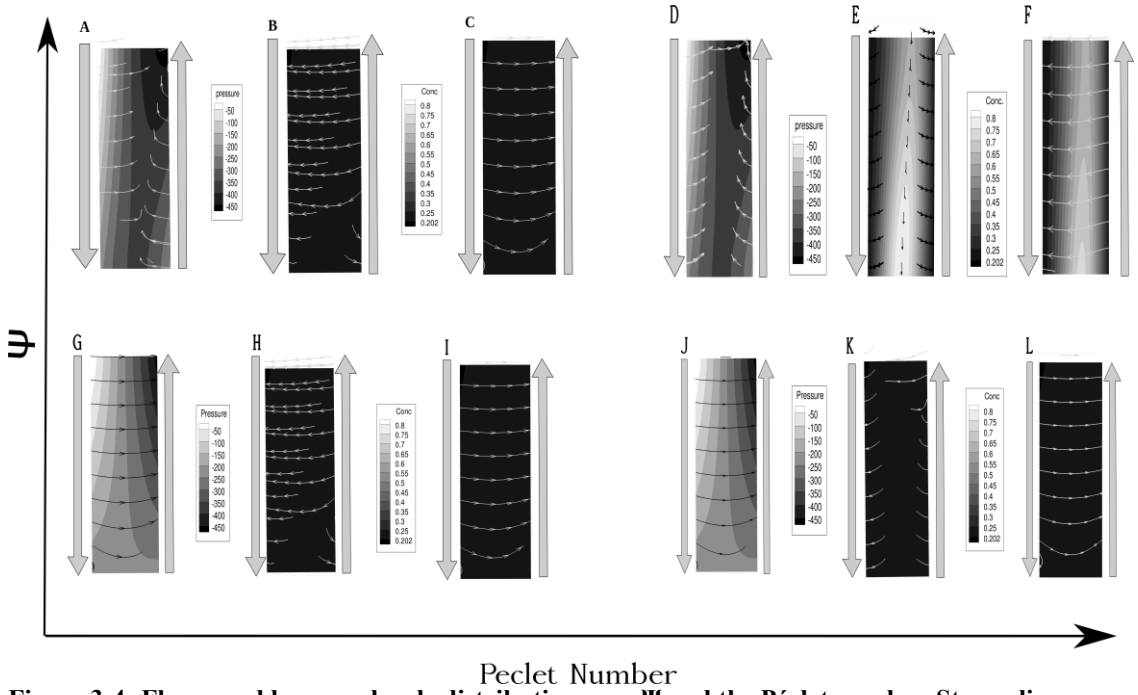

Figure 3-4: Fluxes and large molecule distribution over Ψ and the Péclet number. Streamlines terminate at the top boundary, the basement membrane. A-C) In panels A – C, Pé = 0.34, Ψ = 0.071, δ_{BM} = 0.1, and φ = 0.15. 3A shows the pressure profile and convective flux of the large molecule, B shows the concentration profile and diffusive flux, and C shows the total flux of a large molecule . Here the low Péclet means that despite the high value of Ψ, little accumulation in the mesangial region occurs. Instead, the solute diffuses from the high concentration capillary (afferent) to the low concentration capillary (efferent) as seen in panel C. D-F) In panels D – F, Pé = 2.79, and Ψ = 0.071, δ_{BM} = 0.1, and φ = 0.15. The three panels again show convective flux, diffusive flux, and total flux respectively. Here, the large Péclet number causes extensive mesangial accumulation as convection in from both capillaries dominates. G-I) In panels G-I, Pé = 0.34, Ψ = 0.0028, δ_{BM} = 0.4, and φ = 0.05. Again, the small Péclet number results in no accumulation and the transport is diffusion dominated. J-L) In panels J-L, Pé = 2.79, Ψ = 0.0028, δ_{BM} = 0.4, and φ = 0.05. Here, although the Péclet number is large (which caused extensive accumulation for large values of Ψ), the small value of Ψ causes a convective flow from afferent to efferent. Thus the convection-dominated transport sweeps solutes to the efferent capillary with little mesangial accumulation.

Chapter 4: Discussion and Conclusions

A major contribution of this work is to outline the parameters that influence transport in the glomerular mesangium, and to define their contribution to key dimensionless groups. The model suggests that mesangial transport is strongly influenced by the Péclet number, and, with the inclusion of cell surface receptor binding, also by a dimensionless group that compares receptor reaction rate to diffusion or convection. Macromolecule accumulation in the mesangium has been observed for a long time, and its role in glomerular disease is also well known. However, this model builds a connection between the architecture of the mesangium – its central location, porous matrix, and endothelial connection – and these observations. It also suggests a physical explanation for certain clinical correlations, such as the association of IgA nephropathy with thin basement membranes. The extended model of mesangial transport between glomerular capillaries provides a new dimensionless group, Ψ, which compares mesangial matrix and basement membrane resistances. The ability of this parameter to drastically change the mesangial microenvironment suggests that the mesangial cell's deposition of extra mesangial matrix in response to inflammatory cues may be uniquely counterproductive. This parameter based analysis also gives a new perspective from which to evaluate potential therapeutic strategies. Therapies that directly manipulate these key parameters, e.g. decreasing the Péclet number by increasing matrix digestion or blocking matrix deposition, may be just as effective as attempting to block key cell receptors

Given the sensitivity of the mesangial microenvironment to changes in Péclet number and Ψ, the inflammatory response of mesangial cells and immune cells may aggravate disease progression rather than return the glomerulus to healthy homeostasis. The next step in this work would be to include this dynamic response in the computational model. The current work is limited by the use of steady-state equations at every step. The glomerulus is clearly not a steady-state system. However, the time scale difference between convection and diffusion on the one hand, and matrix deposition/degradation or mesangial cell proliferation on the other hand, would allow a relatively simple model of remodeling that uses the existing steady-state model in a feedback loop with a model of mesangial cell responses to key signals. Such a model of mesangial cell biology, in combination with the model of mesangial transport, could provide key insights into glomerular disease progression.

More broadly, whole areas of mesangial biology and anatomy were ignored in this work. The model does not include any electrical signaling or interaction with the JGA. Mechanical signaling was also ignored, and could also easily be added to the model. Our brief investigation of receptor binding kinetics highlighted its importance, so further incorporation of more detailed receptor kinetics models might improve the validity of this model. Lastly, all this work is based on highly simplified geometries. As has been previously demonstrated (73), while simplified geometric models can provide good overall insight into the basic physics of filtration, incorporating the details of the true glomerular structure can change model outputs significantly. A whole glomerulus model of mesangial transport would eliminate the artificial symmetry boundaries in the

current model, and could give insight into the intra-glomerular to extra-glomerular transport that has been observed. Despite these limitations, the existing model extends our knowledge of transport in the glomerulus, and outlines some key operating spaces in which the mesangium can function.

Bibliography

1. **Abboud HE**. Mesangial cell biology. *Exp Cell Res* 318: 979–85, 2012.
2. **Amore A**, **Cirina P**, **Conti G**, **Brusa P**, **Peruzzi L**, **Coppo R**. Glycosylation of circulating IgA in patients with IgA nephropathy modulates proliferation and apoptosis of mesangial cells. [Online]. *J Am Soc Nephrol* 12: 1862–71, 2001. http://www.ncbi.nlm.nih.gov/pubmed/11518779.
3. **Amsden B**. Solute Diffusion within Hydrogels. Mechanisms and Models. *Macromolecules* 31: 8382–8395, 1998.
4. **Banas B**, **Wörnle M**, **Berger T**, **Nelson PJ**, **Cohen CD**, **Kretzler M**, **Pfirstinger J**, **Mack M**, **Lipp M**, **Gröne H-J**, **Schlöndorff D**. Roles of SLC/CCL21 and CCR7 in human kidney for mesangial proliferation, migration, apoptosis, and tissue homeostasis. *J Immunol* 168: 4301–7, 2002.
5. **Berthelot L**, **Papista C**, **Maciel TT**, **Biarnes-Pelicot M**, **Tissandie E**, **Wang PHM**, **Tamouza H**, **Jamin a.**, **Bex-Coudrat J**, **Gestin a.**, **Boumediene a.**, **Arcos-Fajardo M**, **England P**, **Pillebout E**, **Walker F**, **Daugas E**, **Vrtosvnik F**, **Flamant M**, **Benhamou M**, **Cogne M**, **Moura IC**, **Monteiro RC**. Transglutaminase is essential for IgA nephropathy development acting through IgA receptors. *J Exp Med* 209: 793–806, 2012.
6. **Blantz RC**, **Gabbai FB**, **Tucker BJ**, **Yamamoto T**, **Wilson CB**. Role of mesangial cell in glomerular response to volume and angiotensin II. [Online]. *Am J Physiol* 264: F158-65, 1993. http://www.ncbi.nlm.nih.gov/pubmed/8430826 [16 Jul. 2012].

7. **Blantz RC**, **Konnen KS**, **Tucker BJ**. Angiotensin II effects upon the glomerular microcirculation and ultrafiltration coefficient of the rat. *J Clin Invest* 57: 419–434, 1976.

8. **Branton MH**, **Kopp JB**. TGF-β and fibrosis. *Microbes Infect* 1: 1349–1365, 1999.

9. **Brennan DC**, **Jevnikar a M**, **Takei F**, **Reubin-Kelley VE**. Mesangial cell accessory functions: mediation by intercellular adhesion molecule-1. [Online]. *Kidney Int* 38: 1039–46, 1990. http://www.ncbi.nlm.nih.gov/pubmed/1981601.

10. **Brenner BM**, **Troy JL**, **Daugharty TM**. The dynamics of glomerular ultrafiltration in the rat. *J Clin Invest* 50: 1776–80, 1971.

11. **Burtis CA**, **Ashwood ER**, **Bruns DE**. *Tietz textbook of clinical chemistry and molecular diagnostics*. Elsevier Health Sciences, 2012.

12. **Chary SR**, **Jain RK**. Direct measurement of interstitial convection and diffusion of albumin in normal and neoplastic tissues by fluorescence photobleaching. [Online]. *Proc Natl Acad Sci U S A* 86: 5385–9, 1989. http://www.pubmedcentral.nih.gov/articlerender.fcgi?artid=297627&tool=pmcentrez&rendertype=abstract.

13. **Chauhan VP**, **Stylianopoulos T**, **Martin JD**, **Popović Z**, **Chen O**, **Kamoun WS**, **Bawendi MG**, **Fukumura D**, **Jain RK**. Normalization of tumour blood vessels improves the delivery of nanomedicines in a size-dependent manner. *Nat Nanotechnol* 7: 383–388, 2012.

14. **Choi CHJ**, **Zuckerman JE**, **Webster P**, **Davis ME**. Targeting kidney mesangium

by nanoparticles of defined size. *Proc Natl Acad Sci U S A* 108: 6656–61, 2011.

15. **Clague DS**, **Phillips RJ**. A numerical calculation of the hydraulic permeability of three-dimensional disordered fibrous media. *Phys Fluids* 9: 1562, 1997.

16. **Clauss MA**, **Jain RK**, **Tissues N**. Interstitial Transport of Rabbit and Sheep Antibodies in Normal and Neoplastic Tissues Interstitial Transport of Rabbit and Sheep Antibodies in Normal and Neoplastic Tissues. *Cancer Res* 50: 3487–3492, 1990.

17. **Coelho JB**, **Chien KC**, **Bradley SE**. Measurement of single-nephron glomerular filtration rate without micropuncture. [Online]. *Am J Physiol* 223: 832–9, 1972. http://www.ncbi.nlm.nih.gov/pubmed/5075159 [18 Dec. 2014].

18. **Conrad S a.** Hemodialysis and Hemofiltration. In: *Wiley Encyclopedia of Biomedical Engineering*. John Wiley & Sons, Inc., p. 1–15.

19. **Cosio FG**, **Falkenhain ME**, **Sedmak DD**. Association of thin glomerular basement membrane with other glomerulopathies. *Kidney Int* 46: 471–474, 1994.

20. **Davies M**. The mesangial cell: A tissue culture view. *Kidney Int* 45: 320–327, 1994.

21. **Deen WM**, **Robertson CR**, **Brenner BM**. A model of glomerular ultrafiltration in the rat. [Online]. *Am J Physiol* 223: 1178–83, 1972. http://www.ncbi.nlm.nih.gov/pubmed/4654350.

22. **Deen WM**, **Troy JL**, **Robertson CR**, **Brenner BM**. Dynamics of glomerular ultrafiltration in the rat. IV. Determination of the ultrafiltration coefficient. *J Clin Invest* 52: 1500–8, 1973.

23. **Dember LM**. Amyloidosis-associated kidney disease. *J Am Soc Nephrol* 17: 3458–3471, 2006.

24. **Drumond MC**, **Deen WM**. Structural determinants of glomerular hydraulic permeability. [Online]. *Am J Physiol* 266: F1-12, 1994. http://www.ncbi.nlm.nih.gov/pubmed/8304474.

25. **Duggal R**, **Nada R**, **Rayat CS**, **Rane SU**, **Sakhuja V**, **Joshi K**. Collagenofibrotic glomerulopathy--a review. *Clin Kidney J* 5: 7–12, 2012.

26. **Duque N**, **Gómez-Guerrero C**, **Egido J**. Interaction of IgA with Fc alpha receptors of human mesangial cells activates transcription factor nuclear factor-kappa B and induces expression and synthesis of monocyte chemoattractant protein-1, IL-8, and IFN-inducible protein 10. [Online]. *J Immunol* 159: 3474–82, 1997. http://www.ncbi.nlm.nih.gov/pubmed/9317146 [17 Jul. 2012].

27. **Edwards a**, **Daniels BS**, **Deen WM**. Ultrastructural model for size selectivity in glomerular filtration. *Am J Physiol* 276: F892–F902, 1999.

28. **Elema JD**, **Hoyer JR**, **Vernier RL**. The glomerular mesangium: uptake and transport of intravenously injected colloidal carbon in rats. [Online]. *Kidney Int* 9: 395–406, 1976. http://www.ncbi.nlm.nih.gov/pubmed/181634.

29. **Emancipator SN**, **Rao CS**, **Amore A**, **Coppo R**, **Nedrud JG**. Macromolecular properties that promote mesangial binding and mesangiopathic nephritis. [Online]. *J Am Soc Nephrol* 2: S149-58, 1992. http://www.ncbi.nlm.nih.gov/pubmed/1600131 [16 Aug. 2012].

30. **Gillmore JD**, **Lovat LB**, **Persey MR**, **Pepys MB**, **Hawkins PN**. Amyloid load

and clinical outcome in AA amyloidosis in relation to circulating concentration of serum amyloid A protein. *Lancet* 358: 24–29, 2001.

31. **Gómez-Guerrero C**, **González E**, **Egido J**. Evidence for a specific IgA receptor in rat and human mesangial cells. *J Immunol* 151: 7172–7181, 1993.

32. **Gonzalez-Quintela A**, **Alende R**, **Gude F**, **Campos J**, **Rey J**, **Meijide LM**, **Fernandez-Merino C**, **Vidal C**. Serum levels of immunoglobulins (IgG, IgA, IgM) in a general adult population and their relationship with alcohol consumption, smoking and common metabolic abnormalities. *Clin Exp Immunol* 151: 42–50, 2008.

33. **Gruden G**, **Thomas S**, **Burt D**, **Lane S**, **Chusney G**, **Sacks S**, **Viberti G**. Mechanical stretch induces vascular permeability factor in human mesangial cells: mechanisms of signal transduction. *Proc Natl Acad Sci U S A* 94: 12112–6, 1997.

34. **Gruden G**, **Thomas S**, **Burt D**, **Zhou W**, **Chusney G**, **Gnudi L**, **Viberti G**. Interaction of angiotensin II and mechanical stretch on vascular endothelial growth factor production by human mesangial cells. [Online]. *J Am Soc Nephrol* 10: 730–7, 1999. http://www.ncbi.nlm.nih.gov/pubmed/10203356.

35. **Haraldsson B**, **Nyström J**, **Deen WM**. Properties of the glomerular barrier and mechanisms of proteinuria. *Physiol Rev* 88: 451–87, 2008.

36. **Herrera GA**, **Turbat-Herrera EA**, **Teng J**. Mesangial homeostasis and pathobiology: their role in health and disease. *Exp Model Ren Dis Pathog Diagnosis* 169: 6–22, 2011.

37. **Hiki Y**, **Odani H**, **Takahashi M**, **Yasuda Y**, **Nishimoto A**, **Iwase H**, **Shinzato T**,

Kobayashi Y, **Maeda K**. Mass spectrometry proves under-O-glycosylation of glomerular IgA1 in IgA nephropathy. *Kidney Int* 59: 1077–85, 2001.

38. **Hunt SE**, **Dorfman KD**, **Segal Y**, **Barocas VH**. A computational model of flow and species transport in the mesangium. *Am J Physiol Renal Physiol* 310: F222-9, 2016.

39. **Inkyo-Hayasaka K**, **Sakai T**, **Kobayashi N**, **Shirato I**, **Tomino Y**. Three-dimensional analysis of the whole mesangium in the rat. *Kidney Int* 50: 672–83, 1996.

40. **Kamanna VS**, **Bassa B V**, **Kirschenbaum MA**. Atherogenic lipoproteins and human disease: extending concepts beyond the heart to the kidney. *Curr Opin Nephrol Hypertens* 6: 205–211, 1997.

41. **Keane WF**, **Raij L**. Impaired mesangial clearance of macromolecules in rats with chronic mesangial ferritin-antiferritin immune complex deposition. [Online]. *Lab Invest* 43: 500–8, 1980. http://www.ncbi.nlm.nih.gov/pubmed/7442126.

42. **Kriz W**, **Elger M**, **Lemley K**, **Sakai T**. Structure of the glomerular mesangium: a biomechanical interpretation. [Online]. *Kidney Int Suppl* 30: S2-9, 1990. http://www.ncbi.nlm.nih.gov/pubmed/2259073 [26 Jan. 2012].

43. **Kriz W**, **Elger M**, **Lemley K V**, **Sakai T**. Mesangial cell-glomerular basement membrane connections counteract glomerular capillary and mesangium expansion. [Online]. *Am J Nephrol* 10 Suppl 1: 4–13, 1990. http://www.ncbi.nlm.nih.gov/pubmed/2256475 [26 Jan. 2012].

44. **Kriz W**, **Hosser H**, **Hähnel B**, **Simons JL**, **Provoost AP**. Development of

vascular pole-associated glomerulosclerosis in the Fawn-hooded rat. [Online]. *J Am Soc Nephrol* 9: 381–96, 1998. http://www.ncbi.nlm.nih.gov/pubmed/9513900.

45. **Lai KN**. Pathogenesis of IgA nephropathy. *Nat Rev Nephrol* 8: 275–83, 2012.

46. **Latta H**. An approach to the structure and function of the glomerular mesangium. [Online]. *J Am Soc Nephrol* 2: S65-73, 1992. http://www.ncbi.nlm.nih.gov/pubmed/160013 [26 Jan. 2012].

47. **Latta H**, **Fligiel S**. Mesangial fenestrations, sieving, filtration, and flow. [Online]. *Lab Invest* 52: 591–8, 1985. http://www.ncbi.nlm.nih.gov/pubmed/4010223 [26 Jan. 2012].

48. **Leiper JM**, **Thomson D**, **MacDonald MK**. Uptake and transport of Imposil by the glomerular mesangium in the mouse. [Online]. *Lab Invest* 37: 526–33, 1977. http://www.ncbi.nlm.nih.gov/pubmed/916625.

49. **Lemley K V**, **Elger M**, **Kretzler M**, **Nagata M**, **Sakai T**, **Uiker S**, **Koeppen-Hagemann I**, **Kriz W**. The glomerular mesangium: capillary support function and its failure under experimental conditions. [Online]. *Clin Investig* 70: 843–56, 1992. http://www.ncbi.nlm.nih.gov/pubmed/1450639 [24 Jan. 2012].

50. **Lemley V**, **Lemley K**, **Virginia W**. Structure-Stabilizing Forces in the Glomerular Tuft. *J Am Soc Nephrol* 5: 1731–1739, 1995.

51. **Levick JR**. Flow through interstitium and other fibrous matrices. [Online]. *Q J Exp Physiol* 72: 409–437, 1987. http://www.ncbi.nlm.nih.gov/pubmed/3321140 [9 Dec. 2013].

52. **Linossier M-T**, **Palle S**, **Berthoux F**. Different glycosylation profile of serum

IgA1 in IgA nephropathy according to the glomerular basement membrane thickness: normal versus thin. *Am J Kidney Dis* 41: 558–64, 2003.

53. **Makino H**, **Hironaka K**, **Shikata K**, **Nagake Y**, **Kumagai I**, **Kashihara N**, **Ota Z**. Mesangial matrices act as mesangial channels to the juxtaglomerular zone. Tracer and high-resolution scanning electron-microscopic study. [Online]. *Nephron* 66: 181–8, 1994. http://www.ncbi.nlm.nih.gov/pubmed/8139739 [26 Jan. 2012].

54. **Manil L**, **Davin JC**, **Duchenne C**, **Kubiak C**, **Foidart J**, **Couvreur P**, **Mahieu P**. Uptake of nanoparticles by rat glomerular mesangial cells in vivo and in vitro. [Online]. *Pharm Res* 11: 1160–5, 1994. http://www.ncbi.nlm.nih.gov/pubmed/7971718 [22 Feb. 2012].

55. **Mattana J**, **Singhal PC**. Applied pressure modulates mesangial cell proliferation and matrix synthesis. *Am J Hypertens* 8: 1112–20, 1995.

56. **Mauer SM**, **Fish AJ**, **Blau EB**, **Michael AF**. The glomerular mesangium. I. Kinetic studies of macromolecular uptake in normal and nephrotic rats. *J Clin Invest* 51: 1092–101, 1972.

57. **Michael AF**, **Keane WF**, **Raij L**, **Vernier RL**, **Mauer SM**. The glomerular mesangium. [Online]. *Kidney Int* 17: 141–54, 1980. http://www.ncbi.nlm.nih.gov/pubmed/6991772.

58. **Michael AF**, **Kim Y**. The Glomerular Mesangium. *Am J Kidney Dis* 12: 393–396, 1988.

59. **Migliorini A**, **Ebid R**, **Scherbaum CR**, **Anders H-J**. The danger control concept

in kidney disease: mesangial cells. *J Nephrol* 26: 437–49, 2013.

60. **Morita T**, **Yamamoto T**, **Churg J**. Mesangiolysis: An update. *Am J Kidney Dis* 31: 559–573, 1998.

61. **Moura IC**, **Arcos-Fajardo M**, **Gdoura A**, **Leroy V**, **Sadaka C**, **Mahlaoui N**, **Lepelletier Y**, **Vrtovsnik F**, **Haddad E**, **Benhamou M**, **Monteiro RC**. Engagement of transferrin receptor by polymeric IgA1: evidence for a positive feedback loop involving increased receptor expression and mesangial cell proliferation in IgA nephropathy. *J Am Soc Nephrol* 16: 2667–76, 2005.

62. **Moura IC**, **Benhamou M**, **Launay P**, **Vrtovsnik F**, **Blank U**, **Monteiro RC**. The glomerular response to IgA deposition in IgA nephropathy. *Semin Nephrol* 28: 88–95, 2008.

63. **Myers BD**, **Deen WM**, **Robertson CR**, **Brenner BM**. Dynamics of glomerular ultrafiltration in the rat. VIII. Effects of hematocrit. *Circ Res* 36: 425–35, 1975.

64. **Neal CR**, **Muston PR**, **Njegovan D**, **Verrill R**, **Harper SJ**, **Deen WM**, **Bates DO**. Glomerular filtration into the subpodocyte space is highly restricted under physiological perfusion conditions. *Am J Physiol Renal Physiol* 293: F1787-98, 2007.

65. **Nicholson JP**, **Wolmarans MR**, **Park GR**. The role of albumin in critical illness. *Br J Anaesth* 85: 599–610, 2000.

66. **Nishida Y**, **Oda H**, **Yorioka N**. Effect of lipoproteins on mesangial cell proliferation. *Kidney Int Suppl* 71: S51–S53, 1999.

67. **Okuda T**, **Yamashita N**, **Kurokawa K**. Angiotensin II and vasopressin stimulate

calcium-activated chloride conductance in rat mesangial cells. *J Clin Invest* 78: 1443–1448, 1986.

68. **Olivetti G**, **Kithier K**, **Giacomelli F**, **Wiener J**. Glomerular permeability to endogenous proteins in the rat: effects of acute hypertension. *Lab Invest* 44: 127–137, 1981.

69. **Peti-Peterdi J**. Calcium wave of tubuloglomerular feedback. *Am J Physiol - Ren Physiol* 291: F473–F480, 2006.

70. **Pfeilschifter J**, **Beck K**. Studies on Renal Disorders. Humana Press.

71. **Ramanujan S**, **Pluen A**, **McKee TD**, **Brown EB**, **Boucher Y**, **Jain RK**. Diffusion and convection in collagen gels: implications for transport in the tumor interstitium. *Biophys J* 83: 1650–60, 2002.

72. **Remuzzi A**, **Brenner BM**, **Pata V**, **Tebaldi G**, **Mariano R**, **Belloro A**, **Remuzzi G**. Three-dimensional reconstructed glomerular capillary network: blood flow distribution and local filtration. [Online]. *Am J Physiol* 263: F562-72, 1992. http://www.ncbi.nlm.nih.gov/pubmed/1415586 [24 Jan. 2012].

73. **Remuzzi A**, **Brenner BM**, **Pata V**, **Tebaldi G**, **Mariano R**, **Belloro A**, **Remuzzi G**. Three-dimensional reconstructed glomerular capillary network: blood flow distribution and local filtration. [Online]. *Am J Physiol* 263: F562–F572, 1992. http://www.ncbi.nlm.nih.gov/pubmed/1415586 [24 Jan. 2012].

74. **Remuzzi A**, **Deen WM**. Theoretical effects of a distribution of capillary dimensions on glomerular ultrafiltration. *Microvasc Res* 32: 131–144, 1986.

75. **Ren Y**, **Carretero O a**, **Garvin JL**. Role of mesangial cells and gap junctions in

tubuloglomerular feedback. *Kidney Int* 62: 525–31, 2002.

76. **Riser BL**, **Cortes P**, **Zhao X**, **Bernstein J**, **Dumler F**, **Narins RG**. Intraglomerular pressure and mesangial stretching stimulate extracellular matrix formation in the rat. *J Clin Invest* 90: 1932–43, 1992.

77. **Sakai T**, **Kriz W**. Anatomy and Embryology The structural relationship between mesangial cells and basement membrane of the renal glomerulus. .

78. **Schlondorff D**. The glomerular mesangial cell: an expanding role for a specialized pericyte. *FASEB J* 1: 272–281, 1987.

79. **Schlöndorff D**, **Banas B**. The mesangial cell revisited: no cell is an island. *J Am Soc Nephrol* 20: 1179–1187, 2009.

80. **Scindia YM**, **Deshmukh US**, **Bagavant H**. Mesangial pathology in glomerular disease: targets for therapeutic intervention. *Adv Drug Deliv Rev* 62: 1337–43, 2010.

81. **Shea SM**, **Raskova J**. Glomerular hemodynamics and vascular structure in uremia: a network analysis of glomerular path lengths and maximal blood transit times computed for a microvascular model reconstructed from subserial ultrathin sections. [Online]. *Microvasc Res* 28: 37–50, 1984. http://www.ncbi.nlm.nih.gov/pubmed/6748958 [15 Nov. 2012].

82. **Simonson MS**, **Dunn MJ**. Endothelin-1 stimulates contraction of rat glomerular mesangial cells and potentiates beta-adrenergic-mediated cyclic adenosine monophosphate accumulation. *J Clin Invest* 85: 790–7, 1990.

83. **Sterzel RB**, **Lovett DH**, **Stein HD**, **Kashgarian M**. The mesangium and

glomerulonephritis. *Klin Wochenschr* 60: 1077–1094, 1982.

84. **Sterzel RB**, **Perfetto M**, **Biemesderfer D**, **Kashgarian M**. Disposal of ferritin in the glomerular mesangium of rats. [Online]. *Kidney Int* 23: 480–8, 1983. http://www.ncbi.nlm.nih.gov/pubmed/6188874.

85. **Stevens LA**, **Coresh J**, **Greene T**, **Levey AS**. Assessing kidney function--measured and estimated glomerular filtration rate. *N Engl J Med* 354: 2473–83, 2006.

86. **Stockand JD**, **Sansom SC**. Glomerular mesangial cells: electrophysiology and regulation of contraction. [Online]. *Physiol Rev* 78: 723–44, 1998. http://www.ncbi.nlm.nih.gov/pubmed/9674692.

87. **Swartz MA**, **Fleury ME**. Interstitial flow and its effects in soft tissues. *Annu Rev Biomed Eng* 9: 229–56, 2007.

88. **Takami H**, **Naramoto A**, **Nakazawa K**, **Shigematsu H**, **Ohno S**. Ultrastructure of glomerular mesangial matrix by quick-freeze and deep-etch methods. [Online]. *Kidney Int* 38: 1211–5, 1990. http://www.ncbi.nlm.nih.gov/pubmed/2074664.

89. **Takeda K**, **Meyer-Lehnert H**, **Kim JK**, **Schrier RW**. Effect of angiotensin II on Ca2+ kinetics and contraction in cultured rat glomerular mesangial cells. [Online]. *Am J Physiol* 254: F254-66, 1988. http://www.ncbi.nlm.nih.gov/pubmed/3344808 [15 Nov. 2012].

90. **Takemura T**, **Yoshioka K**, **Aya N**, **Murakami K**, **Matumoto a**, **Itakura H**, **Kodama T**, **Suzuki H**, **Maki S**. Apolipoproteins and lipoprotein receptors in glomeruli in human kidney diseases. *Kidney Int* 43: 918–927, 1993.

91. **Windberger U**, **Bartholovitsch A**, **Plasenzotti R**, **Korak KJ**, **Heinze G**. Whole blood viscosity, plasma viscosity and erythrocyte aggregation in nine mammalian species: reference values and comparison of data. *Exp Physiol* 88: 431–440, 2003.

92. **Wyatt RJ**, **Julian BA**. IgA nephropathy. *N Engl J Med* 368: 2402–14, 2013.

93. **Yamamoto T**, **Mundy C a**, **Wilson CB**, **Blantz RC**. Effect of mesangial cell lysis and proliferation on glomerular hemodynamics in the rat. [Online]. *Kidney Int* 40: 705–13, 1991. http://www.ncbi.nlm.nih.gov/pubmed/1745021.

94. **Yamamoto T**, **Wilson CB**. Quantitative and qualitative studies of antibody-induced mesangial cell damage in the rat. *Kidney Int* 32: 514–25, 1987.

95. **Yao J**, **Morioka T**, **Li B**, **Oite T**. Coordination of Mesangial Cell Contraction by Gap Junction-Mediated Intercellular Ca2+ Wave. *J Am Soc Nephrol* 13: 2018–2026, 2002.

96. **Yao J**, **Zhu Y**, **Morioka T**, **Oite T**, **Kitamura M**. Pathophysiological roles of gap junction in glomerular mesangial cells. *J Membr Biol* 217: 123–30, 2007.

97. **Yasuda T**, **Kondo S**, **Homma T**, **Harris RC**. Regulation of extracellular matrix by mechanical stress in rat glomerular mesangial cells. *J Clin Invest* 98: 1991–2000, 1996.

98. **Zimmerhackl B**, **Parekh N**, **Kücherer H**, **Steinhausen M**. Influence of systemically applied angiotensin II on the microcirculation of glomerular capillaries in the rat. *Kidney Int* 27: 17–24, 1985.

99. OpenStax, Anatomy and Physiology [Online]. OpenStax, CNX. http://cnx.org/contents/14fb4ad7-39a1-4eee-ab6e-3ef2482e3e22@8.81 [8 May

2017].